Aus der Poliklinik für Zahnerhaltung und Parodontologie

der Ludwig-Maximilians-Universität München

Direktor: Prof. Dr. Reinhard Hickel

Polymerization Shrinkage with Light-Initiated Dental Composites

Dissertation

Zum Erwerb des Doktorgrades der Zahnmedizin

an der Medizinischen Fakultät der

Ludwig-Maximilians-Universität zu München

Vorgelegt von

Yu-Chih Chiang

aus

Tainan County, Taiwan

2009

Mit Genehmigung der medizinischen Fakultät

der Universität München

Berichterstatter:	Prof. Dr. Karl-Heinz Kunzelmann
Mitberichterstatter:	Prof. Dr. Andrea Wichelhaus
	Prof. Dr. Wolfgang Plitz
Dekan:	Prof. Dr. med. Dr. h.c. M. Reiser, FACR, FRCR
Tag der mündlichen Prüfung:	20.10.2009

To My Family

My Parents

for their never-ending love, understanding and support

ACKNOWLEDGEMENTS

I would like to express my heartfelt gratitude and appreciation to my supervisor and mentor, Professor Dr. Karl-Heinz Kunzelmann, who always inspires me not only to get insights into science, but also to gain knowledge outside science. His creative guidance and endless dedication gave me great motivation to think differently. His encouragement, enthusiasm, and everlasting friendship made my graduate training at the Ludwig Maximilians University in Munich a memorable and meaningful scientific experience. For helping me get into the field of computational science and learn image processing, I would like to specially thank Dr. Peter Rösch, Professor of FHA-Fachbereich Informatik. I am deeply indebted to Herr Dipl.-Ing. T. Obermeier, Frau E. Köbele and Frau G. Dachs for their encouragement and extensive logistical support. I would also like to express my sincere appreciation to Dr. Indra Nyamaa, Dr. Alp Dabanoglu, Dr. Elisa Magni, Dr. Nicoleta Ilie, Jian Jin, and Elif Öztürk, my colleagues in Tribolabor, and all the people in this department, for their invaluable participation in scientific discussions and generous support.

I would like to specially acknowledge Prof. Dr. Reinhard Hickel, Dean of the Dental School at the Ludwig Maximilians University in Munich, Germany, and Prof. Dr. Chun-Pin Lin, Dean of the School of Dentistry at the National Taiwan University in Taipei, Taiwan, for their constructive comments to this research, for their unconditional support, and for providing me the opportunity to conduct research in Germany. My sincere acknowledgement is extended to Lisa, Prof. Lin's wife, for her warmest encouragement and support, as well as to Dr. Hong-Jiun Chen, my colleague in Taipei, for her editorial skills and tremendous help.

I would like to specially mention Elaine Jane Chua, Thilo Mayer, Yu-Hsueh Chang, and Jimmy Lu for their friendship, never-ending encouragement and support.

Finally, to all those people who I failed to mention here, but in one way or another have been an inspiration to me and provided utmost assistance, I sincerely thank you all.

ABSTRACT

The present work addressed the determination and visualization of the direction and extent of polymerization shrinkage in the light-initiated composite. Hypotheses about the light-cured composite contraction patterns are controversial. With high resolution µCT images, the displacement vector fields are examined and calculated two-dimensionally via an elastic registration algorithm using vector-spline regularization and three-dimensionally with a local rigid registration (block matching) following images segmentation (corresponding traceable fillers in composite). It appears that the light-initiated resin composites do not always shrink toward the light source. Two major contraction patterns were observed: either shrink toward the top-surface (free surface), or toward one side of the cavity wall, in which the bonding was stronger or remained intact. With the proposed methods, it is possible to describe the contraction patterns in great detail. We could demonstrate that the bonding quality to the tooth affects the material movement more than described so far. In addition, the geometry of the cavity also acts as a factor. The continuation of the studies into the interaction of tooth-adhesive-composite indicated the shortcomings and limitations of the current FEA simulation studies. This meant that the assumption of FEA, especially in adhesive systems (i.e., bonding situations and hybridizations), is too perfect and simplificative to interpret the real condition in clinical. The qualitative and quantitative analysis of the shrinkage vector field along with the µCT datasets supply more insight into the shrinkage behavior in real teeth with all their variations of the boundary conditions than with any currently available method. This new approach has the potential to reevaluate and hopefully unify all the currently available hypotheses concerning the extent and orientation of polymerization shrinkage.

TABLE OF CONTENTS

LIST OF FIGURES

Chapter 2

Chapter 3

LIST OF TABLES

General Introduction

1   Composition and Chemical Reaction of Dental Composite

Dental composites are complex materials consist of three major components, organic phase (matrix), inorganic phase (filler), and coupling agent. The resin-based restorative material forms the matrix of the composite material, binding the dispersed glass or silica fillers together via the coupling agent (Craig, 2006).

Organic Phase – Polymer Resin Matrix

The typical polymer matrix used today in commercial composites is still based on either aromatic oligomers (Bis-GMA) or urethane diacrylate oligomer. Bis-GMA (2,2-bis[4-(2-hydroxy-3-methacrylyloxypropoxy)phenyl]propane) is derived from the reaction of one molecular bisphenol-A and two molecular glycidyl methacrylate. The common used urethane diacrylate oligomer is 1,6-bis(methacrylyloxy-2-ethoxycarbonylamino)-2,4,4-trimethylhexane (UDMA). These oligomers contain reactive carbon double bonds (C=C) at each end that can take part in free-radical polymerization reactions, then a highly cross-link polymer is obtained.

Few commercial products utilize the mixture of both Bis-GMA and UDMA. Seeing that their high molecular weights fluids show highly viscous (especially Bis-GMA), they must be diluted with low-viscosity monomers including lower molecular weight difunctional monomers. They are known as viscosity controllers, usually triethyleneglycol dimethacrylate (TEGDMA) or other dimethacrylate monomers, to favor the added filler particles or other additives. However, the low molecular weight methyl methacrylate (MMA) presents higher polymerization

shrinkage (22.5 vol%). Therefore, by raising the molecular weight of MMA from 86.1 g/mole to 514.6 g/mole of Bis-GMA, the shrinkage can be moderated to 8 vol% in the unfilled resin (vanNoort, 2007; Weinmann *et al.*, 2005).

The chemical structures of the common used base and diluent monomers in dental composites are shown as follows:

(MMA)

(Glycidyl methacrylate)

(Bisphenol-A)

(Bis-GMA)

(UDMA)

(TEGDMA)   (Hydroquinone)
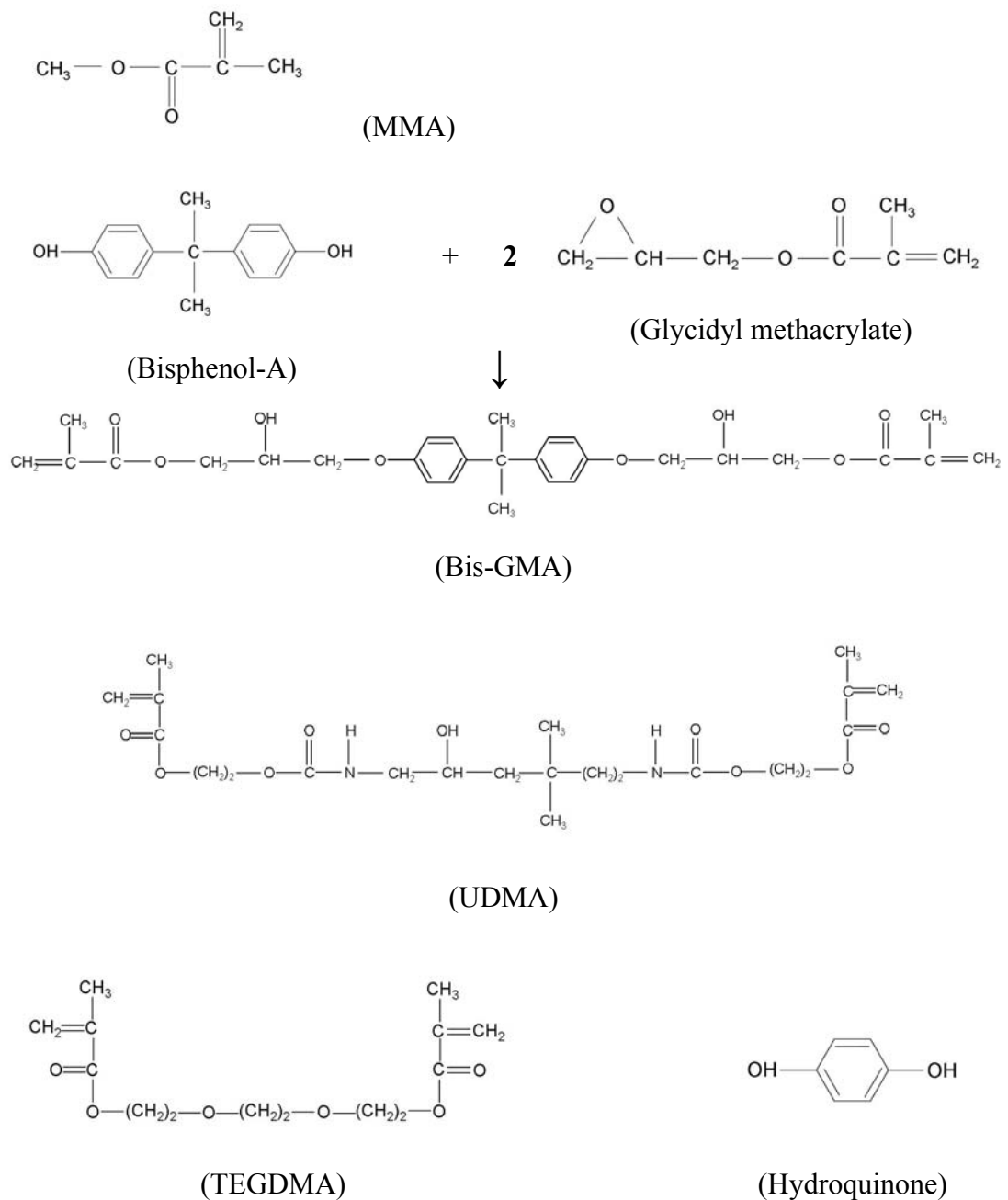
Other organic ingredients in the resin matrix are initiators, accelerators, and inhibitors. Dental composites are formulated to incorporate accelerators and initiators into polymer matrix that may proceed with "self-cure" (chemically activated), "light-cure" (light activated), or a combination of both called as "dual cured" (light and chemically activated) in free-radical polymerization reaction. Free-radical reaction is an addition polymerization and usually occurs with unsaturated molecules comprising carbon double bonds as described by the following equation,

$$n\, CH_2 = CH \quad \xrightarrow{\text{Initiator}} \quad \left[-CH_2 - \underset{\underset{R}{|}}{\overset{\overset{H}{|}}{C}} - \right]_n$$
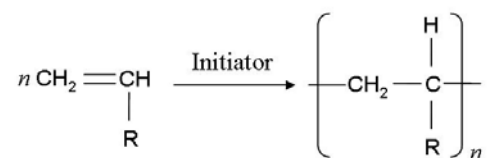
where R stands for any organic group, chlorine, or hydrogen.

The initiator system used in most light-activated dental composites, such as camphoroquinone, added to the monomer in amounts of 0.2-1.0%, needs to absorb light in the wavelength range of 400-500 nm, with peak absorption at 468nm to accomplish the light activation (Strydom, 2005). The reaction is accelerated by the existence of an organic amine comprising a carbon double bond as indicated by the following equation.

(Initiator /accelerator system)   (Activator)

$$Ar_2C = O \quad + \quad RCH_2CH_2NR' \quad \xrightarrow{h\nu} \quad Ar_2\overset{\bullet}{C}-OH \quad + \quad RCH_2\overset{\bullet}{C}HNR'$$

α-diketone   amine   Visual light   free radicals
e.g. camphoroquinone   (460nm-480nm)
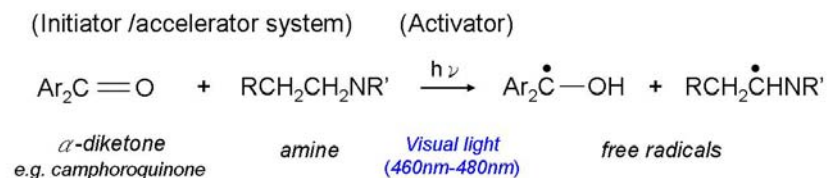
Due to the color demand, other photo-activators, which also may be used in some dental composites, react at peak absorption around 430 nm. In addition, small amount of inhibitors, such as 0.1% hydroquinone (or less), are used to prevent the dimethacrylate-based resin composite from premature polymerization, which remain an adequate long shelf life for the monomer.

In order to achieve an optimal polymerization rate, cross-linking and mechanical properties, several investigations have undertaken the evaluation of the relative effect of the different monomers in bis-GMA/UDMA/TEGDMA mixtures (Asmussen and Peutzfeldt, 1998; Chowdhury *et al.*, 1997; Inai *et al.*, 2002; Skrtic and Antonucci, 2007).

As polymerization shrinkage persists in these methacrylate-based resin composites like a major impediment, dental research switched the resin matrix to a novel ring-opening monomer, which is a combination of siloxane and oxirane moieties and therefore named Silorane (Eick *et al.*, 2007; Ilie *et al.*, 2007; Weinmann *et al.*, 2005). Based on the ring-opening polymerization, Silorane-based resin composite materials present a low-shrinkage feature. The most difference of the polymerization process in Silorane is that metharylates-based materials are cured by the "radical intermediates", whereas oxiranes are polymerized through the "cationic intermediates", as shown in the following illustrations (Weinmann *et al.*, 2005).
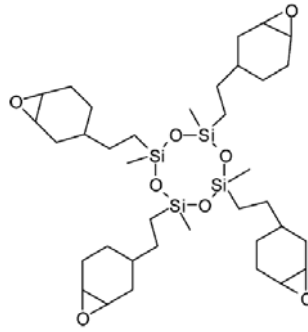
(Chemical structure of Silorane monomer)
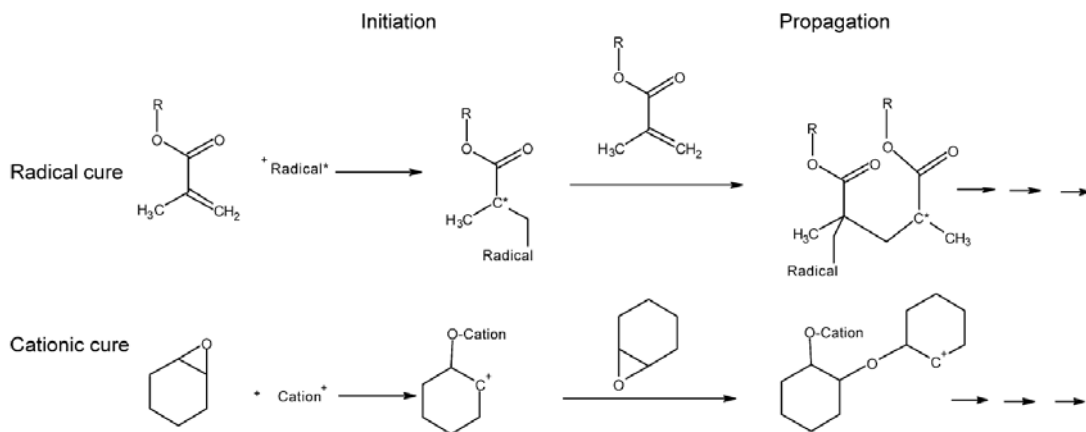
Inorganic Phase – Filler Particles

The dispersed filler particles in polymer matrix in contemporary dental composites may comprise several inorganic materials such as quartz (fine particles), silica glasses containing barium or strontium, other silica-based glass fillers including colloid silica (microfine particles), lithium-aluminum silicate glass, or zirconia-silica nanoclusters and silica nanoparticles which are produced by a sol-gel process (nanotechnology). The role of incorporated fillers offers five potentially major benefits (vanNoort, 2007):

(1). The considerable amount of polymeric matrix is relatively decreased by incorporating large amount of inorganic fillers and the fillers do not go in for the polymerization process, in consequence, the polymerization shrinkage is much decreased (Roulet *et al.*, 1991).

(2). Mechanical properties such as hardness and compressive strength can be enhanced.

(3). By adding the glass fillers, the high thermal expansion coefficient of methacrylate based monomers ($\sim$ 80ppm/$^{\circ}$C) could be quite compensated to obtain a similar expansion coefficient to tooth tissue (8-10ppm/$^{\circ}$C).

(4). Various aesthetic features such as color, translucency, and fluorescence can be moderated by the given fillers.

(5). The glass fillers can act as carriers to resist secondary caries with fluoride-containing fillers, and to exhibit radiopacity by using heavy metals like barium or strontium.

Table 1 summarized a useful classification of dental composites based on the particle size, shape, and distribution of fillers. A comparable data of Silorane-based resin composite, against methacrylate-based resin composite, was also added in the table.

Table 1. Classification of Direct Resin Composite Restoratives

Composite classification	Filler content		Volume shrinkage (%)	Average particle size (μm)
	Weight %	Volume %		
Hybrid	74-87	57-72	1.6-4.7	0.2-3.0
Nanohybrid	72-87	58-71	2.0-3.4	0.4-0.9 (macro)
	–	–	–	0.015-0.05 (nano)
Microfills	35-80	20-59	2-3	0.04-0.75
Flowables	40-60	30-55	4-8	0.6-1.0
Compomers	59-77	43-61	2.6-3.4	0.7-0.8
Silorane-based*	50-70	–	0.94-0.99	0.015-5

* Data was obtained from (Puckett *et al.*, 2007; Weinmann *et al.*, 2005)

Coupling Agent – Connector

Since polymeric matrix is hydrophobic, whereas the silica-based filler is hydrophilic, a durable connection must form between these two phase to obtain an acceptable properties of resin composite during polymerization. Bonding is achieved by the manufacturer treating the surface of the fillers with a coupling agent (i.e. filler silanization) before incorporating them into polymeric matrix. The most common coupling agent, called silane (3-methacryloxypropyltrimethoxysilane), is kind of organic silicon compounds containing difunctional group. During the activation of the silane on the glass filler, the methoxyl groups hydrolyze to hydroxyl groups that react with the adsorbed moisture or –OH groups on the filler. The carbon double bonds of this silane react with the polymer matrix during setting, accordingly forming a bond from the hydrophilic filler through the coupling agent to the hydrophobic polymer

matrix. A typical formula and the reaction of silane coupling agent were depicted as follows.
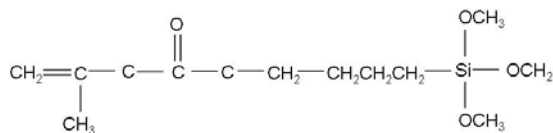
(3-methacryloxypropyltrimethoxysilane)
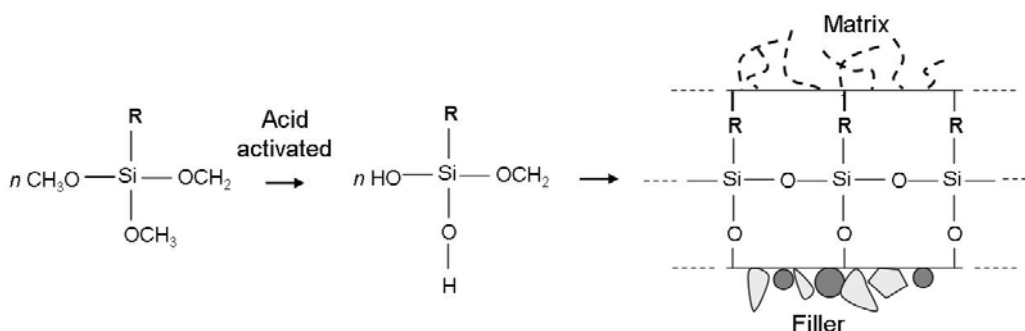
2   Clinical Relevance

Dimethacrylate-based (Bis-GMA) resin composites were introduced in the 1960s as a possible substitute for acrylic resin in dentistry (Bowen, 1963). With the increasing demand for esthetic perfection and physical properties dental composites have been considerably expanded their clinical applications. In the past ten years, the improved performances of resin composites have encouraged more clinicians to select resin-based composites for posterior restorations as an alternative to amalgam (Jordan and Suzuki, 1991; Leinfelder, 1993; Ottenga and Mjor, 2007; Roulet *et al.*, 1991). Nevertheless, dimethacrylate-based resin composites still demonstrate some negative or questionable aspects: wear resistance, surface roughness, handling property, proximal contact and contouring or sculpturing, and marginal adaptation, and polymerization shrinkage, for example.

The excessive wear loss of composite restorations could be observed below the enamel margin, or proximal contacts with the adjacent tooth in class II restorations. Consequential open proximal contacts or mesial drifting of tooth would occur. This phenomenon may arise from a combination factors, including polymer or filler composite, filler size, and filler-polymer matrix binding quality, especially in earlier resin composite systems (Kusy and Leinfelder, 1977; Labella *et al.*, 1999). The containing large quartz fillers (>100μm diameter) were easily plucked from the composite surface during polishing procedures or mastication. The protruding filler particles well bond to polymer matrix may also lead to rough surface and make polish the surface difficult, because the hardness of them are much higher than matrix, and then the surface of the restorative grew into a roughness that was dependent on the size of the fillers. We can put this way that the wear process of dental composites is one accelerated by environmental softening of the composites (Wu *et al.*, 1984). Other researchers also reported that some degradation of the filler/matrix interface and the reduction in the fracture toughness, as has been observed clinically, occur after long-term exposure of dental composites to certain solvents used as food-simulating liquids (Ferracane and Marker, 1992).

Surface roughness may also collect organic debris that results in discoloration. However, the improved filler particles, silanization technique and developing nanotechnology allow current resin composites comprising a combination of filler particles that are much smaller in diameter (hybrid composite or nano-composite) and allow higher filler loadings and fillers-polymer matrix binding, and maintaining a smooth surface finish (Jung *et al.*, 2007; Xia *et al.*, 2008). Thus, the problem of wear, surface roughness, and discoloration, which are primarily related to the resin

composite materials, seem no longer to be critical clinical challenges. However, this doesn't indicate that the improvements in these properties would not be necessary.

3   Polymerization Shrinkage vs. Polymerization Shrinkage Stress

Polymerization shrinkage is a large concern region of research on dental composites: methods to minimize the total amount of shrinkage, how to accurately calculate it, how to measure the direction of mass movement (vector), and how to evaluate and manage the stress effects it originates are the subjects of most recent studies (Ferracane, 2008; Giachetti *et al.*, 2006; Lutz *et al.*, 1986b; Park *et al.*, 2008). To inaugurate the polymerization contraction behavior of dental composite restoration, it's necessary to have an insight into the mechanisms related to the properties and characteristics of resin composites.

As monomers cross-link with adjacent monomers, the mobile monomer molecules move closer and convert into covalent bonds like a polymer network, incurring the volumetric shrinkage or called bulk contraction (Venhoven *et al.*, 1993). In general, a majority of the shrinkage takes place before the solidification, called gel-point or pre-gelation phase, while the mass of materials is still plastic enough to flow. Presumably in the early plastic stage, only chain formation occurs and cross-linking is not yet at full reaction allowing molecules to move into new positions. At a later stage (post-gelation), the polymerization process accompanies a rapid increase in stiffness (elastic modulus or Young's modulus) of the materials during solidification (Davidson and de Gee, 1984). Clinically, the mass movement of resin composite is hindered or inhibited by the constraint of the material bonded to the tooth substrate. In virtue of the subsequent solidification, the material is rigid enough

to resist sufficient plastic flow to compensate for the original volume. Therefore, the shrinkage manifests itself as stress, known as the so called "polymerization shrinkage stress" (Chen *et al.*, 2001; Davidson and Feilzer, 1997; Giachetti *et al.*, 2006). It was hypothesized that the magnitude of stress directly depends on differences in degree of conversion, volumetric shrinkage, elastic modulus, and the ratio of co-monomers (Goncalves *et al.*, 2008; Pfeifer *et al.*, 2008). The polymerization process of resin-based composite related to gelation, shrinkage, elastic modulus, and shrinkage stress was illustrated in Fig. 1.
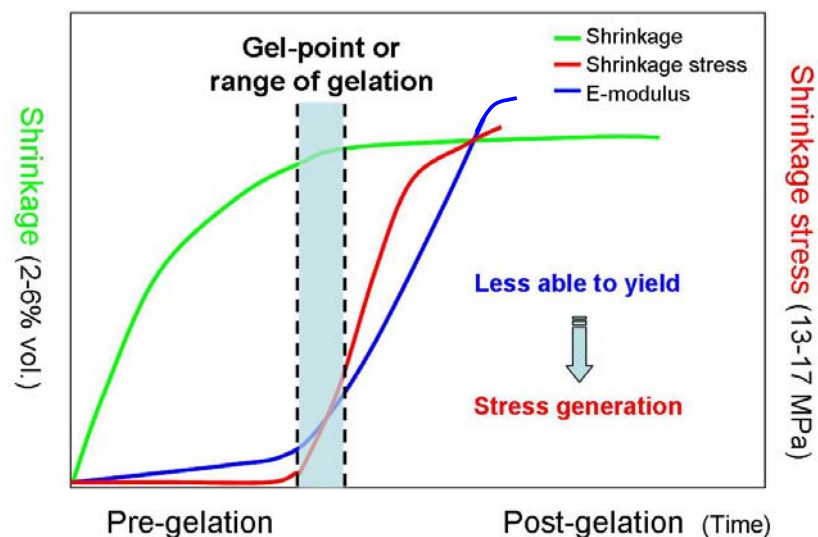
Figure 1. A schematic diagram of the brief relationship among the shrinkage, elastic modulus, and shrinkage stress.

4 Clinical Outcomes Related to Polymerization Shrinkage

Polymerization shrinkage is one of the most critical concerns when dental clinicians place the direct resin composite restoration. In vitro measurement of the polymerization shrinkage (strain) vary from 0.2% to 2% linearly (Hansen, 1982b;

Rees and Jacobsen, 1989), and from 1.5% to 6% volumetrically (Bowen, 1963; Kleverlaan and Feilzer, 2005) for the dimethyacrylate-based composites, depending on their specific formulation of commercial products. Though shrinkage strain is an interesting fundamental value, in a clinical situation, this value changes due to the adhesive process, and shrinkage stresses are generated instead. If the bonding strength between the tooth structure and resin composite is efficient to resist the mass contraction during polymerization, stress occurs when the cross-linking density prevents the accommodation of shrinkage strain by viscoelastic flow of the polymer, except on the free surface area (Davidson, 1986; Feilzer et al., 1990). With the levels of bonding strengths currently achievable and the different configuration of restoration cavity (C-factor), these stresses accompanied are reported to vary from 5MPa to 17MPa (Alomari et al., 2007; Feilzer et al., 1987; Watts and Cash, 1991; Zanchi et al., 2006).

Polymerization shrinkage stress generated by contraction of the resin composite restoration is most competitive on the interface of restoration/tooth (Dauvillier et al., 2000; Davidson and Feilzer, 1997). This situation often leads to the heavily pre-stressed restorations which may give rise to detrimental clinical consequences such as the follow (Giachetti et al., 2006; Versluis et al., 1996):

(1) Deformation: the shrinkage stress is conducted to the tooth substance and causes tooth deformation, which may bring on enamel crack or fracture, cracked cusps, and cuspal strain and displacement (Asmussen and Jorgensen, 1972; Bouillaguet et al., 2006; Meredith and Setchell, 1997; Suliman et al., 1994). Larger restoration may cause lower stress levels in the interface but increase stress in the surrounding tooth structures if the cavity walls are thin enough to deform

(Versluis *et al.*, 2004).

(2) Failure risk during loading: if the bonding strength is strong enough to resist gaps formation, the stress transferred inside the resin composite mass would be generated and exited. Either initiation of micro-crack in composite or compliance of the surrounding structures could be occurred during hardening (Davidson *et al.*, 1991). However, the former case would not occur clinically since the compliance or deformation sufficiently relieves the setting stress to a lower level before cohesive or adhesive failure. The residual stresses are maintained by the whole elastic deformation of the tooth-composite complex. This phenomenon, accordingly, implies a risk of failure during the functional loading (mastication) (Davidson and Feilzer, 1997; Versluis *et al.*, 2004).

(3) Failure of tooth-restoration interface: if contraction forces exceed the bonding strength at the interface, the consequential stress has the potential to initiate failure of the composite/tooth interface as so-called adhesive failure (Davidson *et al.*, 1984). The resulting interfacial gaps may lead to staining, marginal leakage (Barnes *et al.*, 1993; Bowen, 1963), post-operative sensitivity (Camps *et al.*, 2000; Pashley *et al.*, 1993), and secondary caries (Ferracane, 2008; Garberoglio and Brannstrom, 1976).

For the progression of secondary caries, a simplistic commentary that begins with marginal gaps developing marginal staining, advancing on microleakage along the cavity wall, and finally on secondary caries was often described. The correlation between the polymerization contraction behavior of dental composite restorations and their clinical outcomes is not yet directly proved, but, it is true that the diagnosis of

secondary caries is the main reason given for the replacement of dental composites in the past 20 years (Bernardo *et al.*, 2007; Deligeorgi *et al.*, 2001; Manhart *et al.*, 2004; Qvist *et al.*, 1990; Sarrett, 2005). It is also true that these polymer-based materials accompany the inevitable 1.5%-6% volumetric contraction during polymerization. A summarized data from practice-based studies on causes of restoration failure in resin-based composites was demonstrated in Table 2.

Table 2. Main Cause Related to Restoration Failure in Resin Composites		
Year: Author	Data on restoration failure	Replacement of restorations
2007: Bernardo et al.		Percent of replacements due to secondary caries: amalgam 3.7%; composite 12.7% (In 3-surface composite restoration: 31.1%)
2001: Burke et al.	>39% restorations are replacements	29% placed due to secondary caries
2001: Deligtorgi et al. (review of 10 studies)		Secondary caries main reason; marginal degradation, discoloration, bulk fracture, wear more likely with composite
2000: Mjör et al.		Secondary caries main reason
2000: Deligeorgi et al.	48% (Manchester) and 82% (Athens) are restorations placed for primary caries	33% (Manchester) and 54% (Athens) replaced due to secondary caries
1999: Burke et al.	51% of restorations are replacement	22% placed due to secondary caries; percent of replacements due to secondary caries: amalgam 46%; composite 40%; glass ionomer 40%
1999: Burke et al.		30% of restorations placed due to secondary caries of previous restoration; secondary caries main reason regardless of material
1998: Mjör and Moorhead		Percent of replacements due to secondary caries: amalgam 56%; composite 59%

5   Factors Contributed to Polymerization Shrinkage or Generated Stresses

Monomer System

Although higher molecular weight monomers (e.g. Bis-GMA, Bis-EMA, and UDMA) in place of lower molecular weight monomers (e.g TEGDMA) would increase the viscosity and reduces the contraction of resin composite, the stress is indeed inevitable and perhaps higher stress was lingered due to its higher mechanical property formed. Some researcher emphasized on developing new composite formaulations such as new silorane and oxirane chemistries with volumetric shrinkage approaching 1% (Weinmann *et al.*, 2005). Theses expanding monomers, based on expoxy and spiro-orthocarbonate-based resins (e.g. 2,3-bis methylene spiro-orthocarbonate) can expand in volume during polymerization through a double ring-opening process in which two bonds are cleaved for each new bond formed (Stansbury, 1992). The shrinkage associated with the common methacrylate-based monomers can be offset by applying the resulting expansion (Millich *et al.*, 1998).

Concentration of Initiators and Inhibitors vs. Degree of Conversion

During the polymerization of multifunctional monomers for dental composite materials, the typical final double-bond conversions are in the range of 55%-75% (Barron *et al.*, 1992; Kalipcilar *et al.*, 1991; Sideridou *et al.*, 2002). The polymerization rate has also been shown to influence the contraction stress generated in resin composites. In that case, a higher levels of inhibitor (BHT) may reduce curing rate, contraction stress and rate of stress formation in experimental composites, but not compromise the final degree of conversion (Braga and Ferracane, 2002; Schneider

et al., 2009). Other investigations demonstrated that the degree of conversion and reaction of kinetics can be regulated by varying the concentrations of initiators (Atai and Watts, 2006; Watts and Cash, 1991).

Filler Content and Elastic Modulus

Both the magnitude of the shrinkage and the modulus of the elasticity of the resin composite directly affect the polymerization shrinkage stress. The space occupied by filler particles in polymer matrix cannot participate in the curing shrinkage. Therefore, increasing the ratio of the filler/composite results in decreasing the polymerization shrinkage, but also increases the elastic modulus. Based on the Hooke's Law, the higher the elastic modulus becomes, the higher the stress gains in the same amount of shrinkage. For example, micro-filled composite, which includes less filler particles than hybrid composites, shows greater shrinkage, but tend to create lower stress than hybrids; likewise nano-filled and highly-filled hybrid composites have been shown to exhibit higher shrinkage stress than such a hybrid composite with a lower filler content.

Furthermore, nanofiller particles (smaller than 100nm) create such a high surface/volume ratio that provide an extensive surface interactions with polymerizing monomers to induce internal stresses by constraining the mobility of the molecules during polymerization, especially in case of the silanized filler particles. To relieve the internal stress, non-treated nanofiller particles or non-bonded nanofiller particles treated with non-functional silane coupling agent (no C=C double bonds) was incorporated into resin composite, thereby the interaction between the filler surface and the forming polymer was minimized without compromising the mechanical

properties (Condon and Ferracane, 1998).

Cavity Geometry (C-factor)

In order to describe the relationship between confinement conditions and stress values, Feilzer *et al.* created and defined the term "cavity configuration factor" (C-factor) as the ratio of bonded surfaces (restrained) to unbonded surfaces (free) of the rein composite restoration (Feilzer *et al.*, 1987). A schematic representation of the relation between the corresponding C-values and the stress from their cylindrical experimental samples was shown as below.
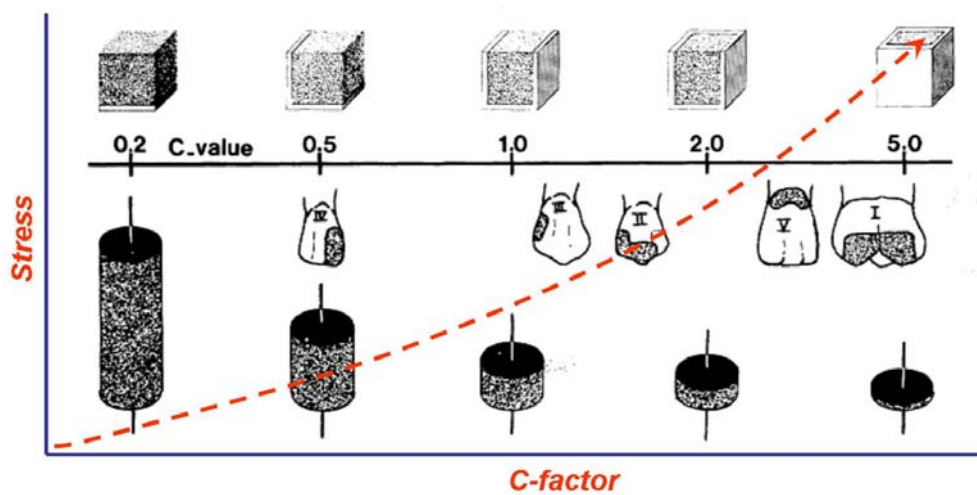
With cylindrically shaped specimens (a near-zero compliance testing system), the authors found that higher C-factors corresponded to higher stress values. For example, if two Class I cavities have the same volume but a different shape design, the shallower and wider cavity will present a lower C-factor than the deeper and narrower one. The less the restoration is restrained (bonded) by the cavity walls, the less shrinkage stress interference there will be. That is to say, the free surface (unbonded)

18

area allows the stress to be compensated for by the flow of the mass of restorative materials, especially in pre-gel phase.

However, it is not possible to transfer the concept of the C-factor directly to the clinical situation since tooth cavity preparation reveals a much more complex geometry (i.e. regional difference of dental substrate or the effects on intrinsic wetness) than the specimens used in mechanical testing experimentally, and in consequence the tooth-adhesive-composite system exhibits a very heterogeneous stress distribution (Hipwell *et al.*, 2003; Kinomoto *et al.*, 1999).

Hygroscopic expansion

The effect of polymerization shrinkage is somewhat tempered by the phenomenon of water sorption and its resulting hygroscopic expansion, which causes resin composite to swell with time and may offset some residual elastic stresses (Bowen, 1963; Feilzer *et al.*, 1990). This compensation mechanism would also be affected by the particular configuration of the cavity. Neither the original shrinkage stress nor the hygroscopic expansion will be constant all over the restoration. Thus, a new stress or an "expansion stress" will be somewhere generated (Feilzer, 1989; Kemp-Scholte and Davidson, 1990). No matter how this hygroscopic compensation mechanism relieves the polymerization shrinkage, water sorption of resin composite results in a series of negative consequences such as degradation, soften and color instability (Giachetti *et al.*, 2006; McKinney and Wu, 1985).

6   Clinical Strategies to Manage Shrinkage Stress Development in Composites

Incremental Placement Technique

It is widely accepted that applying the resin composites layer by layer instead of using a bulking technique will minimize the shrinkage stress. There are several incremental techniques were recommended to reduce the effect of polymerization contraction such as Facio-lingual Layering (vertical), Gingivoocclusal Layering (horizontal), Wedge-shape Layering (oblique), Successive Cusp Build-up Technique, Centripetal Build-up Technique, and Three-site Technique using light-reflecting wedges (Bichacho, 1994; Liebenberg, 1996; Lutz *et al.*, 1986a; Summitt *et al.*, 2006; Tjan *et al.*, 1992).

Two major factors support this concept: application of a small volume of materials and minimal contact with the opposing cavity walls (C-factor) during polymerization. It is ascertained that smaller volume of resin material produces less amount of shrinkage. Theoretically, each layer is compensated by the next, and the resulting polymerization shrinkage is less damaging while the free surface is likely to enhance stress relief by allowing more flow. In other words, if an infinite number of layers were applied into cavity, the magnitude of polymerization shrinkage would be insignificant. However, the movement of mass material in polymerization will not stop immediately after the light-initiation. Only 70-85% of shrinkage occurred immediately following light-initiation, and after 5 minutes approach up to 93% (Sakaguchi *et al.*, 1992), that is to say, a substantial strain from the polymerization in the first layer could still be under development during the application of the last increment. There is currently no laboratory or clinical data to answer definitely the question of what is the optimal placement technique. In terms of the reduction of shrinkage or shrinkage stress, the layering techniques may be questioned. A finite element analysis (FEA) study indicated that incremental filling techniques increase

more deformation of the restored tooth more than the bulk technique (Versluis *et al.*, 1996). However, this does not mean that the incremental techniques should be overthrown. The ascendancies for applying the resin composite in layers involve easier handling, better sculpturing of the restoration, and the promotion of the degree of conversion. By contrast, the bulk light-curing method will lead to a lower degree of conversion deep inside the restoration since the intensity curing light decreases as it penetrates deeper in to the bulk composite restoration.

Stress Absorbers

The use of resilient or deformable liners as stress-absorbing layer between the hybrid layer and the filled resin composite has been promoted to partially relieve the stress development and evaluated by numerous investigators. The so-call "flowable composites" have been shown to present low viscosity, high polymerization shrinkage values and inferior mechanical properties as a result of their lower filler content. The higher shrinkage could potentially cause more stress on the adhesive interface, whereas their lower elastic modulus would in turn generate less stress if compared to traditional filled composites. These low stiffness flowable composite could be provided to act as a stress absorber, presumably by deforming to absorb some of the restorative composite shrinkage strain, whereby the bulk contraction of the restoration can obtain some freedom of movement from the adhesive sides (Braga and Ferracane, 2002; Cunha *et al.*, 2006). In addition, a liner with more rubbery property placed under composite restoration has been reported to reduce gap formation in cavities (Dewaele *et al.*, 2006). Glass ionomers or resin-modified glass ionomers have also been used as a liner or base under composite restoration. The role of stress relief is facilitated by the deformation or internal failure of the weaker ionomer material,

whereas both the bond to tooth and the resin composite are preserved (Kemp-Scholte and Davidson, 1990; McLean *et al.*, 1985). Moreover, the glass ionomer establishes a reliable gap-free chemical bond to both dentin and composite, and reduces the volume of resin composite in the cavity (consequentially reduces the volumetric contraction). The unfilled resin adhesive applied in thick layers under composites has been also reported to reduce stresses significantly (Kemp-Scholte and Davidson, 1990). It seems that stress-absorbing layers play an important role reducing the polymerization shrinkage stress under composite restoration; however, it is still debated and the clinical evidence proving enhanced success with this method has not been presented (Braga and Ferracane, 2002; Ferracane, 2008).

Alternatives of Light Curing Method

An increase in inhibitor concentration for initial curing conduct a decrease in polymerization speed and thus in shrinkage stress without affecting the final conversion rate of composite. Lower light irradiance to 250mW/cm^2 has been shown to significantly improve marginal adaptation as compared with irradiating the resin composite at either 450 mW/cm^2 or 650 mW/cm^2 (Feilzer *et al.*, 1995; Unterbrink and Muessner, 1995). In order to establish a rapid and readily performed clinical technique, many researchers are seeking a method that combines low initial intensity and short exposure times. These so-called "soft-start curing" methods can be sorted into stepped-curing, ramped-curing or pulse-delay technique (Strydom, 2005; Summitt *et al.*, 2006).

Ramped-curing technique:

Ascent irradiance is performed from a low to a high level over a period of approximately 10 seconds, to slow the initial reaction.

Stepped-curing technique:

Curing starts at low but constant irradiance, namely, around 150 to 300 mW/cm^2, for between 2 and 10 seconds; for the remainder of the exposure time, irradiance is increased to between 600 and 800 mW/cm^2 (Bouschlicher *et al.*, 2000; Kanca and Suh, 1999).

Pulse-delay technique:

This technique incorporates a waiting period between exposures. Curing starts at short dose of low irradiance, around 3-5 seconds at 100-250mW/cm^2, and is then stopped for a given period ranging from a few seconds to a few minutes (waiting period); light is then applied at high irradiance (800 to 1,200mW/cm^2) in 1 or more pulses (Chan *et al.*, 2008; Hofmann and Hunecke, 2006; Pfeifer *et al.*, 2006). The greatest reduction in polymerization shrinkage stress (as much as 34%) could be achieved with a waiting period between pulses of 3 to 5 minutes (Sharp *et al.*, 2003).

Regardless of the name, "stepped", "soft-start", "pulse-delay" or "ramped" curing technique, the underlying principle is similar: initial cure at lowered irradiance to initiate the polymerization reaction at a slower rate to provide sufficient polymer cross-linking formation on the composite surface while delaying the gel point in the lower layers until a final high-intensity polymerization is initiated (Alomari *et al.*, 2007; Summitt *et al.*, 2006).

It is likely that the interfacial integrity could be preserved with low light irradiance since it elongates the viscoelastic stage of the setting material. Most authors identified with these techniques, since, although it does not diminish polymerization shrinkage (Yap *et al.*, 2001), it generates less stress (Ernst *et al.*, 2000; Pereira *et al.*, 1999) less marginal leakage (Kanca and Suh, 1999), fewer gaps (Mehl *et al.*, 1997; Obici *et al.*, 2002), and better interface (Gallo *et al.*, 2005), while ensuring mechanical properties as good as those achieved with conventional high-irradiance techniques. However, some studies reported that this soft-start technique does not actually improve the effect of polymerization shrinkage (Bouschlicher *et al.*, 2000; Friedl *et al.*, 2000; Sahafi *et al.*, 2001). This result may be explained by the different concentrations of photo-initiators; therefore, the gel point should be anticipated even with a soft-start polymerization. On the other hand, clinically, it is challenging to decide the optimal level of light energy which leads to the best relationship among conversion degree, mechanical properties, and contraction stress. In addition, it's known that over-exposing the composite to light-activation might induce the risk of marginal and interfacial debonding, as well as a heat build-up within the tooth (Braga and Ferracane, 2002). Therefore, although rational lower light irradiance is indeed beneficial to slow the polymerization reaction, no specific recommendation can be made for a specific technique.

7   Polymerization Shrinkage Measurements in Dentistry

Throughout the years, numerous approaches tried to analyze the polymerization shrinkage and its consequences for the shrinkage stress. During the process of monomer development, chemists are usually more interested in the free volumetric shrinkage which can be measured for example using the method of Archimedes, the

mercury dilatometer (de Gee *et al.*, 1981), linometer (de Gee *et al.*, 1993) or by optical monitoring of volume changes (i.e. AccuVol – Bisco) (Sharp *et al.*, 2003). Dental researchers, on the other hand, are more interested in the shrinkage stress. Shrinkage stress is measured for example using a tensilometer (Davidson *et al.*, 1984), a Stress-Strain-Analyzer testing machine (Chen *et al.*, 2001), stress-strain-gauges (Sakaguchi *et al.*, 1991) or the method of Watts and Cash (Watts and Cash, 1991). However, none of these measurements match the clinical situation because most setups are an idealization and simplification of the true conditions. The simulation of the shrinkage behavior with a finite element analysis (FEA) is an alternative approach to collect more insight into the clinical situation, but is limited by some necessary assumptions for the FEA (Versluis *et al.*, 1998).

In vitro experiments, using extracted teeth, based on dye penetration and quantitative marginal gap analysis (Roulet *et al.*, 1991) seem to be the most valid approaches to evaluate and compare different material combinations "composite – dentin bonding agent" and methods to minimize the consequences of curing contraction. However, since the introduction of the hydrophilic dentin bonding agents the dye penetration technique is of limited use because these hydrophilic dentin bonding agents are stained by the dye themselves and it is very hard to differentiate the true gaps from the stained dentin bonding layers. The quantitative margin analysis is also very time-consuming. In addition, it is hard to predict how deep a gap extends into the dentin, for it is not only the length but also the depth of a gap which can negatively affect the vitality of a tooth. Therefore, an experimental model in association with real clinical situations is mandatory to assess the direction and amount of the light-initiated dental composite due to polymerization.

8   Hypotheses

The X-ray micro-computed tomography device (μCT) has been recently used to analyze the interface of the dentin-adhesive-composite (De Santis *et al.*, 2005) and to examine the 3-D marginal adaptation in light-cured resin composite restoration (Kakaboura *et al.*, 2007).

The direction of the polymerization shrinkage, so called shrinkage vector, has long been of interest, but still remained unclear. In order to disclose the complex of composite-adhesive-tooth, it is necessary to understand the direction and amount of the mass movement. Though the polymerization shrinkage value of the composite materials may rather smaller, the availability of high resolution μCT (Clementino-Luedemann *et al.*, 2006; Sun and Lin-Gibson, 2008) makes it now possible to get real 3-D information about what happens in a cavity during polymerization.

It appears that the real direction and amount of the composite material due to light-initiated polymerization can reflect on the acquired μCT images. The hypotheses in this study are: (1) The polymerization shrinkage vectors could be visualized by the registration of corresponding markers in μCT images, which were recorded before and after curing. (2) Light-initiated dental composites do not always shrink toward the light. We assumed that certain radiolucent glass fillers can be regarded as the traceable markers as well as identified from the μCT images. In addition, they must be silanized and incorporated into composite matrix to ensure the durable connection.

In this study, we try to develop the reliable registration methods which can

two-dimensionally (Chapter 1) or three-dimensionally (Chapter 2) visualize the real shrinkage vectors by experimentally analyzing the μCT images. The 2-D and 3-D results will back up with each other to test the reliability themselves. With these developed methods, we can also apply to evaluate the effects of different dentin bonding agents on the shrinkage behavior (Chapter 3).

Chapter 1

Shrinkage Vector Visulization in Dental Composite Materials – A X-Ray Micro-Computed Tomography Study

1.1 Background and Significance

The orientation of polymerization shrinkage vectors is a fundamental set of data in predicting marginal integrity and stress distribution (Asmussen and Jorgensen, 1972; Cabrera and de la Macorra, 2007; Versluis *et al.*, 1998). The magnitude and direction in which this shrinkage occurs can be described by so-called shrinkage vectors (Watts and Cash, 1991). The magnitude of the shrinkage vectors depends on the chemical composition of the composite material (Anseth *et al.*, 1996; Ferracane, 2008; Stansbury, 1992) and the degree of conversion (Braga and Ferracane, 2002), which is affected by the effective light intensity and curing time (Asmussen and Peutzfeldt, 2001; Dietschi *et al.*, 2003; Koran and Kurschner, 1998). The direction of shrinkage is influenced by the cavity geometry (Asmussen and Jorgensen, 1972; Davidson and Feilzer, 1997; Feilzer *et al.*, 1987), the adherence to the cavity surface (beginning of the bonding area) (Cho *et al.*, 2002) and the position of the light source (Asmussen and Peutzfeldt, 1999; Lutz *et al.*, 1986b; Palin *et al.*, 2008; Versluis *et al.*, 1998).

An important hypothesis in dental literature is that light-cured resin-composites shrink toward the light source and self-cured resin-composites shrink towards the center of mass (Asmussen and Peutzfeldt, 1999; Hansen, 1982a). However, there is little evidence regarding the direction of the polymerization shrinkage vectors of

28

light-initiated resin composite. Finite element analysis (FEA) was used to visualize the shrinkage vectors (Versluis et al., 1998). This theoretical study concluded that light-initiated resin composites do not shrink toward the light, instead the cavity shape and bonding quality seem to be more important predictors. Finite element simulations are based on a number of assumptions which may or may not represent the real situation. Therefore, the outcome of FEA studies should be validated experimentally.

The availability of high resolution X-ray micro-computed tomography apparatus (μCT) (Clementino-Luedemann et al., 2006; Sun and Lin-Gibson, 2008) makes it now possible to acquire real 3-D information within a cavity during light-initiated resin composite polymerization, and to examine the 3-D marginal adaptation and interface of the dentin-adhesive-composite (De Santis et al., 2005; Kakaboura et al., 2007).

The aim in this part of this study was to develop an experimental method which combines μCT datasets with images registration approach to determine and visualize the direction and amount of polymerization shrinkage vectors in order to gain insight into the consequences of curing contraction.

1.2 Materials and Methods

1.2.1 Synthesis of experimental resin composite

To visualize the material movement, radiolucent spherical glass fillers with an average particle size of 40-70 μm in diameter (Sigmund Linder GmbH, Warmensteinach, Germany), were used as traceable markers. The dimethacrylate based flowable resin composite (Tetric® EvoFlow, Ivoclar, Vivadent AG, Schaan/Liechtenstein, Switzerland) was selected for this first experiment in order to obtain shrinkage values which can be clearly identified with the given μCT resolution. The glass beads were silanized to ensure a durable connection to the composite. The silanization procedure was based on the alkaline method (Chen and Brauer, 1982). The total amount of glass beads added to the composite was approximately 1.5 wt%. The materials used for this study are listed in the Table 1-1.

1.2.2 Specimen preparation

A total of six non-carious human permanent molars were collected and stored in distilled water containing 0.2% thymol at 4˚C. Their cusp tips were removed to obtain a flat surface. The flat surface ensured a consistent and unimpeded access for light curing. In each tooth, a Class I cylindrical cavity, 3 mm in depth and 6 mm in diameter, was prepared. The prepared tooth was embedded in the micro-CT sample holder (15/13.5mm in outer/inner diameter, 43mm in height) (Fig. 1-1).

The teeth were divided into two groups. In the control group, the dentin surface was not pre-treated with a dentin bonding agent, while a self-etching dentin bonding agent (Table 1-2) was applied to the second group. The group without bonding was

30

introduced as a negative control.

The tooth restored with the experimental resin composite was covered with a radiolucent dark cap to avoid hardening of the resin composite during the μCT measurements. The restoration was digitized before and after light-curing (40 s, 950 mW/cm^2 light intensity, 8 mm light-tip diameter, LED SmartLight$^®$ PS, Dentsply/Caulk, DE, USA).

1.2.3   X-ray micro-computed tomography

A high resolution X-ray micro computed tomography (μCT 40, Scanco Medical AG, Basserdorf, Switzerland) was used to analyze the material movement due to the curing contraction of the light-curing resin composite (Fig. 1-2). The settings for the μCT were: acceleration voltage 70 kVp and cathode current 114 μA. The samples were scanned with 8 μm resolution using an integration time of 300 ms and were never removed from the μCT attachment. Therefore, it was possible to compare the measurements before and after light-curing by selecting corresponding slice numbers of the data stacks. The 3-D data before and after polymerization were subjected to an image analysis. A flow chart of obtaining the digital 3-D data before image registration is shown in Fig. 1-3.

1.2.4   Images processing and registration

1.2.4.1   Image pre-processing

The total size of the acquired data sets was typically around 2 GB (16 bit binary data), which makes it nearly impossible to handle the files on desktop computers with

a 32 bit operating system. In order to reduce the amount of data, the images were cropped to display only the composite restoration (Fig. 1-4A). In addition, the data were converted to 8 bit binary images, because only the shape information was included for the current evaluation. If necessary, an additional downsampling step was included (factor 2 in x, y, z direction by averaging using the mean). Image preprocessing was performed with ImageJ (Rasband, 2005). A custom plug-in was written to import the μCT data sets. The cropped volumes of interest were filtered with a median filter (radius 2) to reduce noise in the data sets.

The image size after pre-processing was 500 x 500 x 250 with an isotropic voxel size of 16 μm. The subsequent image registration is based on the pre-processed images (Fig. 1-4B).

1.2.4.2 Image processing and deformation field examination

Corresponding slices of the data stacks were used to determine the displacement of the glass beads after polymerization. The displacement vector field was calculated with an elastic registration algorithm using vector-spline regularization (Arganda-Carreras *et al.*, 2006; Sorzano *et al.*, 2005).

To register two images, we assume that one of the images (source image, $I_s(x, y)$, I = image, s = source, the image I is a function of x and y) is an elastically deformed version of the other (target image, $I_t(x, y)$, t = target) such that

$$I_s\big(g(x, y)\big) = I_t\big(x, y\big),$$

where $g(x, y)$ is the deformation field as a function of x and y. Elastic fields can be

expressed in terms of B-splines as

$$g(x,y) = \left(g_1(x,y), g_2(x,y)\right)$$

$$= \sum_{k.l \in Z^2} \begin{pmatrix} C_{1,k,l} \\ C_{2,k,l} \end{pmatrix} \beta^3 \left(\frac{x}{s_x} - k\right) \beta^3 \left(\frac{y}{s_y} - 1\right)$$

where β^3 is the B-spline of degree 3, $C_{k,l}$ are the B-spline coefficients, and s_x and s_y are scalars (sampling steps) controlling the degree of detail of the representation of the deformation field.

To ensure the deformation flow to the correct direction, we manually added landmarks at the centre of traceable glass beads in both the source (uncured resin composite) and the target image (cured resin composite). An example of image processing is shown in Fig. 1-5.

1.2.5 *Deformation change calculation and examination*

The vector fields serve as a graphical representation of the deformation. The vector length (V_l) due to deformation change was obtained via the pixel-to-pixel correspondence as

$$V_l = \sqrt{\left(x_s - x_t\right)^2 + \left(y_s - y_t\right)^2}$$

where (x_s, y_s) and (x_t, y_t) are the coordinates of the source and target images.

We determined the deformation changes along the longitudinal planes, one along the y-axis and another along the z-axis. In addition, transversal planes along the x-axis

33

were selected every 0.5 mm from the top surface of the restoration to a depth of 2 mm to permit the interpretation of the results (Fig. 2).

For a quantitative comparison, the vector length values were summarized as a histogram. The standard deviation (SD) of the histogram, the skewness and the kurtosis were calculated to characterize the distribution of the deformation vectors. In addition, specimens were longitudinally cut to observe the marginal adaptation with a scanning electron microscope (ZEISS GEMINI® FESEM, SUPRA™ 55VP, Carl Zeiss SMT AG, Oberkochen, Germany).
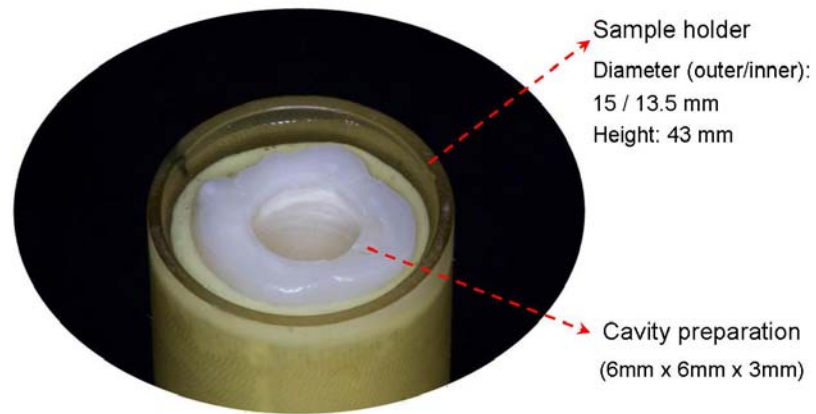
Figure 1-1. The embedded and prepared tooth in the sample holder. The tooth cusp tip was removed to obtain a flat surface. The flat surface ensured a consistent and unimpeded access for light curing. The tooth was embedded in the sample holder of the micro CT attachment. The surrounding distill water was used to prevent the tooth from over-dry.

(A)

(B)
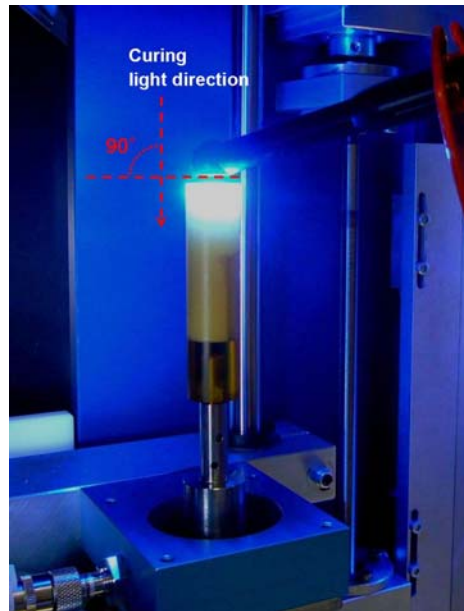
Figure 1-2. (A) A high resolution X-ray micro-computed tomography (µCT 40, Scanco Medical AG, Basserdorf, Switzerland) was used to analyze the material movement. (B) The restoration was digitized before and after light-curing (40 s, 950 mW/cm^2 light intensity, 8 mm light-tip diameter, LED SmartLight$^®$ PS, Dentsply/Caulk, DE, USA).
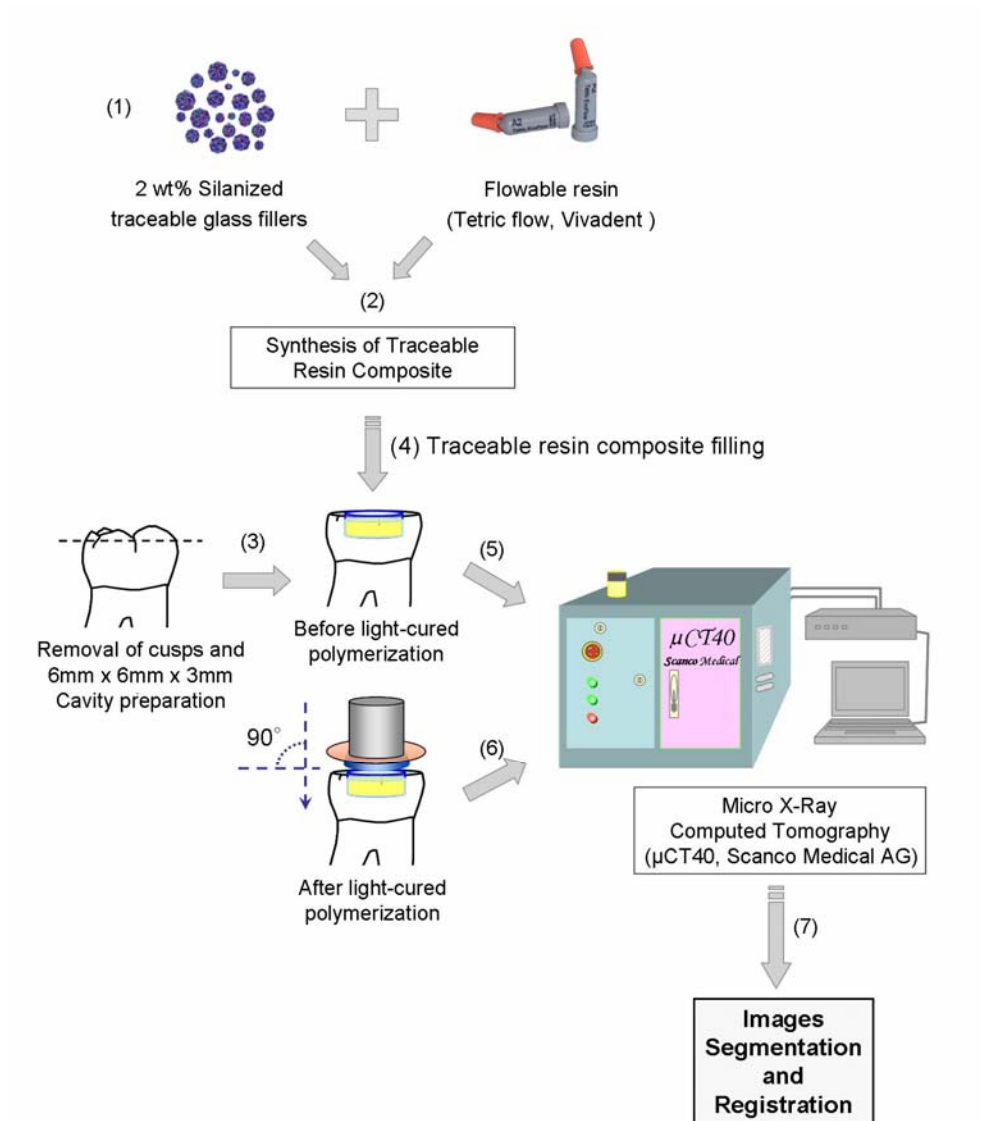
Figure 1-3. A flow chart of obtaining the digital 3-D data before and after polymerization. A radiolucent and dark cap (not drawn) was used to cover the restoration to avoid hardening of uncured resin composite during μCT measurements. The numbers in brackets indicate the sequence of the performed steps.

(A)
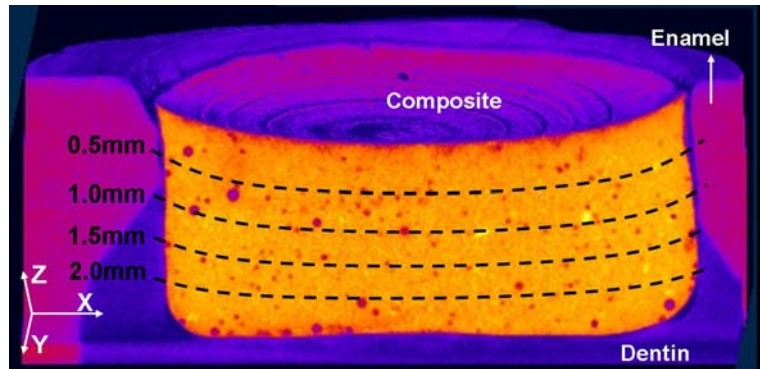
(B)
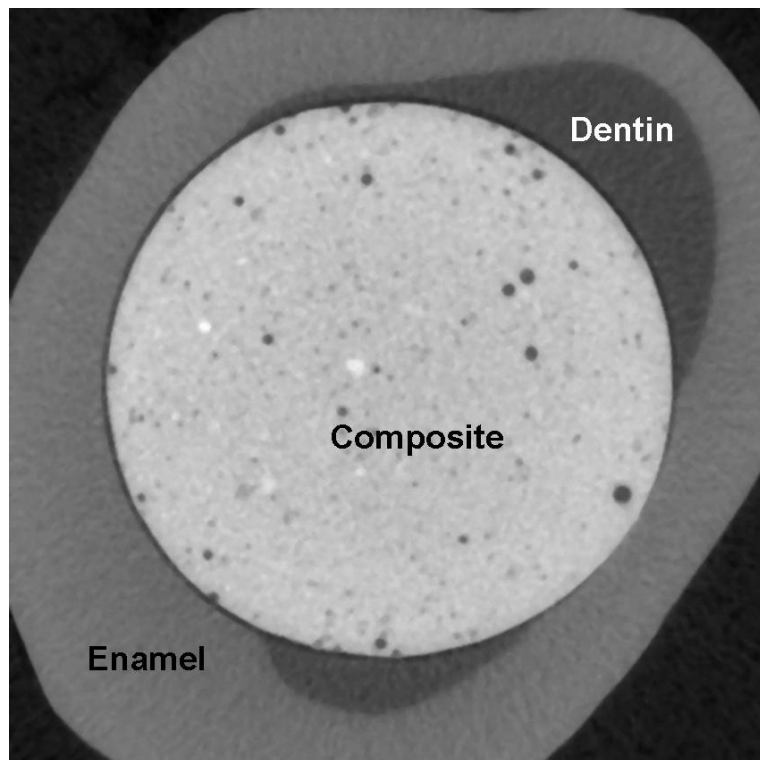
Figure 1-4. (A) 3-D image reconstruction: Based on the 3-D data, the restoration is visualized and the horizontal planes, which were analyzed for the 2D elastic registration, are displayed together with the axis orientation which is referred to in the text. (B) The horizontal slices are oriented along the xy-plane. Detachment can be observed on the upper left cavity wall. The subsequent image registration is based on the pre-processed images.

(A)
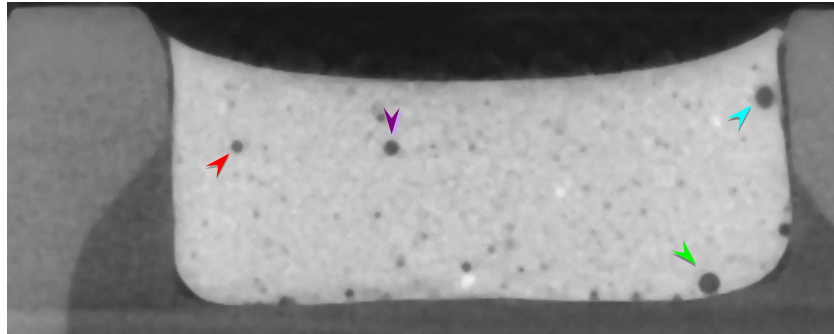
(B)
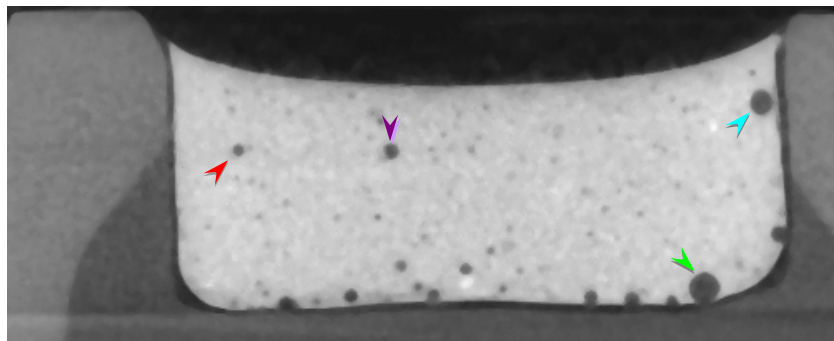
Figure 1-5. Example of image processing (sagittal view; yz-plane). (A) Source image, uncured resin composite. Arrowheads pointed out the selected traceable glass beads. (B) Target image, cured resin composite. The corresponding traceable markers were pointed out by arrowheads.

(C)
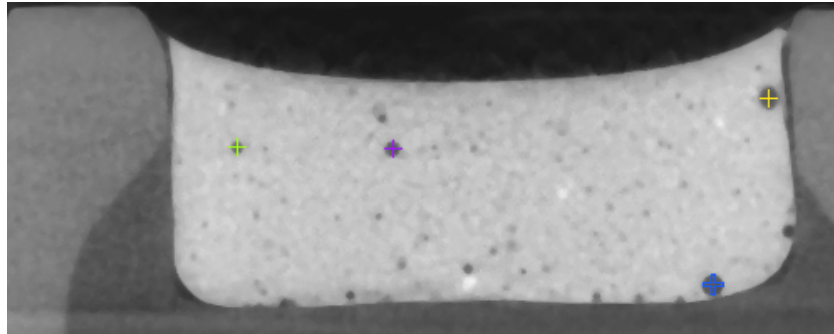
(D)
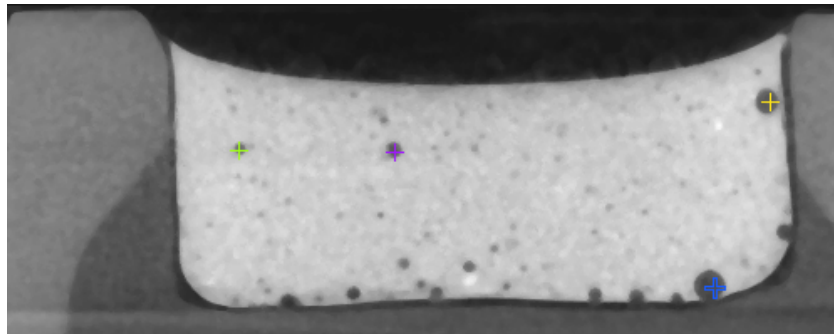
(E)
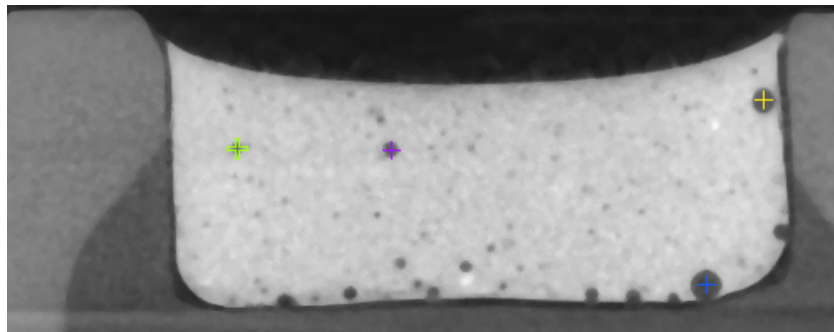
Figure 1-5. Example of image processing (sagittal view; yz-plane). (C) Add landmarks appeared in crosses in the centre of apparent traceable glass beads of source image. (D) The added landmarks are automatically placed in the same position of target image. (E) Drag the landmarks into the centre of corresponding glass beads in target image.

(F)
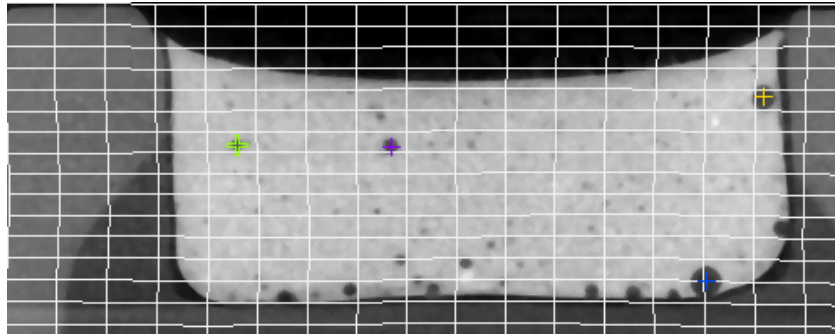
(G)
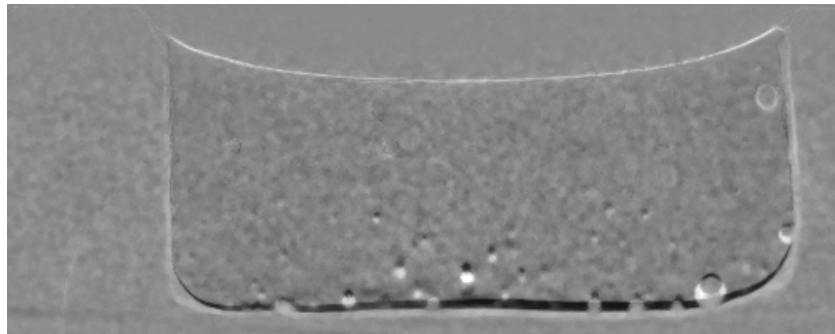
(H)
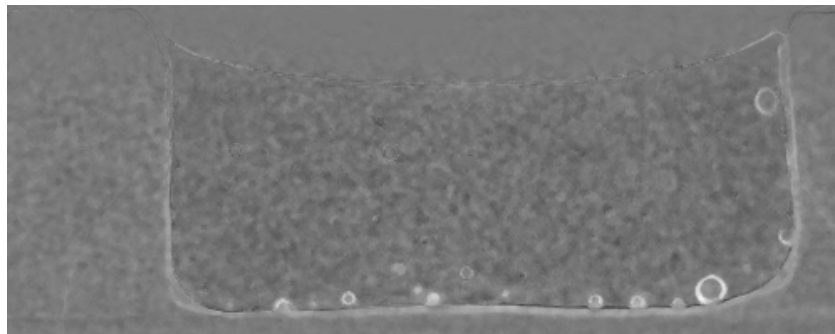
Figure 1-5. Example of image processing (sagittal view; yz-plane). (F) Mapping of a current grid from the target to source, superimposed to the target image. (G) Image processing and registering. (H) Difference source image, error image shown during the process. The corresponding traceable glass beads have accurately mapped.

(I)
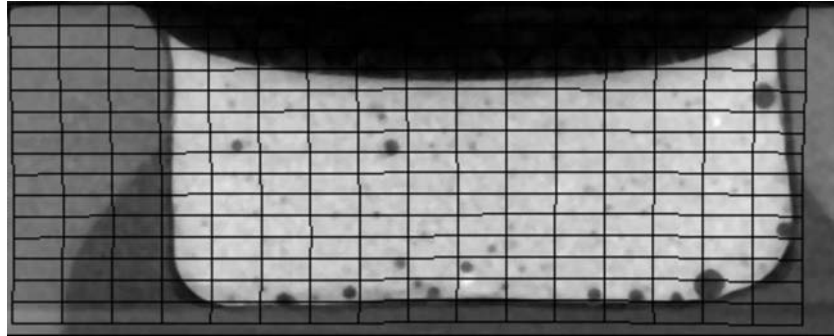
(J)
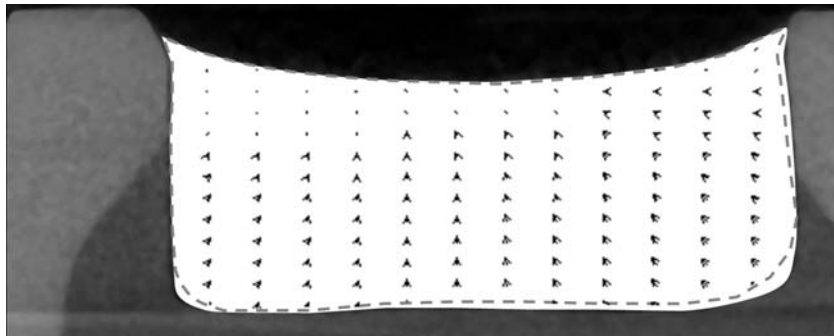
Figure 1-5. Example of image processing (sagittal view; yz-plane). (I) Original source image (uncured resin composite) with the deformation grid. (J) Displacement field is obtained from the elastic registration: Superimposed to the output source-target image of registered target image. Deformation displays as a vector field due to the mass movement of polymerization shrinkage. Dotted line (cured resin composite) showed the deformed shape after light-curing of resin composite.

Table 1-1. Composition of Experimental Resin Composite Used in this Study

Brand name	Composition	Batch No.	Manufacturer
Tetric® EvoFlow (Flowable resin)	Matrix: dimethacrylates (38 wt%) Fillers: barium glass, ytterbium trifluoride, highly dispersed silicon dioxide, mixed oxide and copolymer (62 wt%) Others (< 1 wt%) Particle sizes of the inorganic fillers: 40 nm to 3000 nm	LOT: J21884	Ivoclar Vivadent AG, Bendererstrasse 2, FL - 9494 Schaan, Principality of Liechtenstein
Glass Beads (Radiolucent spheres, as traceable markers)	SiO_2 (72.50 wt%), Na_2O (13.00 wt%), CaO (9.06 wt%), MgO (4.22 wt%), Al_2O_3 (0.58 wt%) Diameter: 40-70 μm 8% more than 100μm	Art No: 5211	Sigmund Linder GmbH, Warmensteinach , Germany

Table 1-2. Composition of Dentin Bonding Agent Used in this Study

Brand name	Composition	Batch No.	Manufacturer
Adper^{TM} Prompt L-Pop (Self-Etch Adhesives)	Liquid 1 (red blister): Methacrylated phosphoric esters, bis-GMA, initiators based on camphorquinone, stabilizers Liquid 2 (yellow blister): Water, 2-Hydroxyethyl methacrylate (HEMA), polyalkenoic acid, stabilizers	LOT: D2691319369	3M, ESPE St. Paul, MN

1.3 Results

The glass spheres, which were added to the flowable composite, can be easily identified in the µCT images (Fig. 1-4). They appear as the digital correlate of radiolucent spheres of different diameters in the 3-D datasets. The centers of the spheres were used as the input for an elastic registration algorithm using vector-spline regularization. The deformation field after the elastic registration clearly showed the displacement of the glass beads after curing (Fig. 1-6 and 1-7). The arrows represent the displacement vectors. Vectors have two basic properties, a direction and a length. In our case the direction of the vectors represents the direction of the movement of the glass spheres while the length of the vector stands for the length of the movement. The interpretation of the results is easier if one considers the two types of information of the vector field separately: the general orientation and the average length of the vectors.

1.3.1 *Orientation of the displacement field*

Fig. 1-6 shows the unbonded control group. The composite still adheres to one cavity wall (left side, Fig. 1-6A) and is pulled from the other walls. Thus a compensatory gap is formed at the non-adhering cavity areas. The displacement field perpendicular to the z-axis confirms this observation (Fig. 1-6B).

We observed two different outcomes in the bonded restoration group. Subgroup one (similar enamel thickness at the vertical walls): the predominant orientation of the displacement vector field is toward the top-surface of the restoration (Fig. 1-7A) while at the bottom of the cavity a radiolucent area is visible. Subgroup two (different

enamel thickness): the translucent area at the bottom of the cavity does not exist (Fig. 1-7B). The main orientation of the deformation vector field is toward the bottom of the cavity. There, the composite is in tight contact with the tooth surface. Overall, one side usually adheres to the cavity wall, while a radio-translucent layer is frequently visible at the interface between the composite and the dentin wall.

In the unbonded group, the displacement vectors adjacent to the top-surface of the restoration are oriented towards the center of the cavity (Fig. 1-6A). In contrast, the direction of the displacement vectors of the bonded group depends on the subgroup and can orient toward the bottom of the cavity (Fig. 1-7B) or in the opposite direction, toward the outside of the cavity (Fig. 1-7A); the latter condition results in a slightly higher restoration surface after curing.

1.3.2   *Deformation changes*

The amount of movement depends on adhesion to the cavity wall. Fig. 1-8 shows the distribution histogram of all vector length values for all teeth within the same groups. The histogram of the bonded group can be described with the statistical parameters (unit = pixels): mean = 8.5, standard deviation = 9.7, skewness = 4.8 and kurtosis = 35.9. The same parameter set for the unbonded group was: mean = 8.1, standard deviation = 5.8, skewness = 2.5 and kurtosis = 15.5. The histogram maximum of the unbonded group was smaller than the histogram maximum of the bonded group. In addition to the primary maximum, the bonded group exhibits a second maximum at 80 pixels, representing longer displacement vectors. A certain proportion of vectors were even less than one pixel in the bonded group, which is equivalent to no mass movement.

1.3.3   *Scanning electron microscopy*

The displacement vectors fields (shrinkage behavior) of the light-initiated resin composite were confirmed by the SEM examinations. The SEM observations showed the silanized glass beads which we added into the composite established a well-bond with the matrix (Fig. 1-8). In the bonded restoration of subgroup1 specimen, the composite material close to the superficial enamel created an optimal marginal seal (Fig. 1-9A). However, the bond to dentin substrate at the bottom of the cavity failed after polymerization, which allowed the material to shrink toward the top surface of the restoration (Fig. 1-9B). The resulting shrinkage gaps were about 40-100 μm. Likewise, in bonded subgroup 2 specimen, a compensatory gap occurred at one side of the lateral cavity wall due to the stronger adherence to opposite sides (Fig. 1-10A). The thicker enamel sheltered the underlay dentin from the polymerization shrinkage and contributed to the integrity of the adhesion at the bottom of the cavity (Fig. 1-10B).

(A)
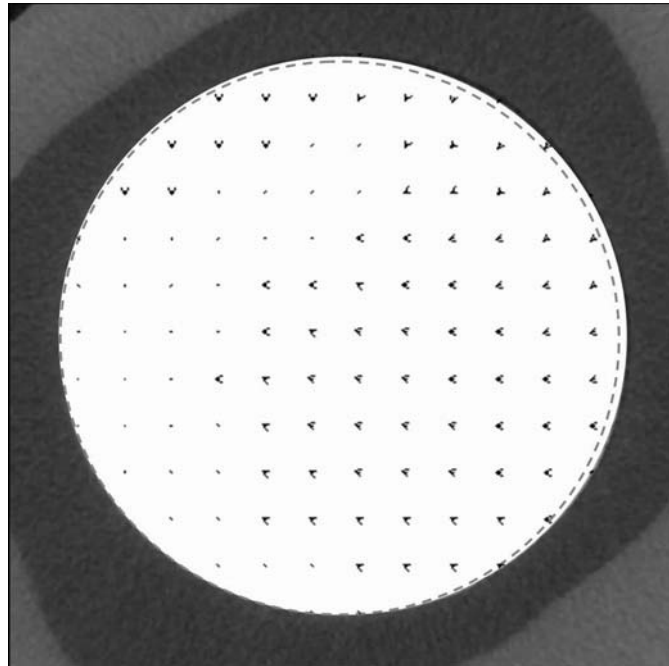
(B)
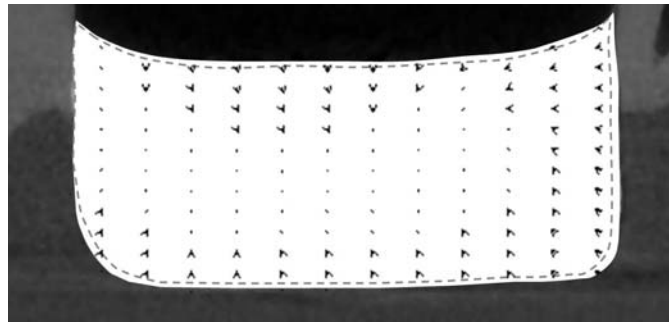
Figure 1-6. Shrinkage vectors distribution of the unbonded restoration.

(A) Slice along the xy-plane: Most of the vectors in this displacement vector field point to the left side of the figure, where the displacement vector length is very small or zero.

(B) Slice along the xz-plane: This slice along the xz-plane shows that the restoration adheres to the enamel margin on the left top of the cavity. The restoration is detached from the other walls of the cavity. Most of the vectors point to the center of mass. Where the restoration is still attached to the enamel margin the displacement vector length is very small.

(A)
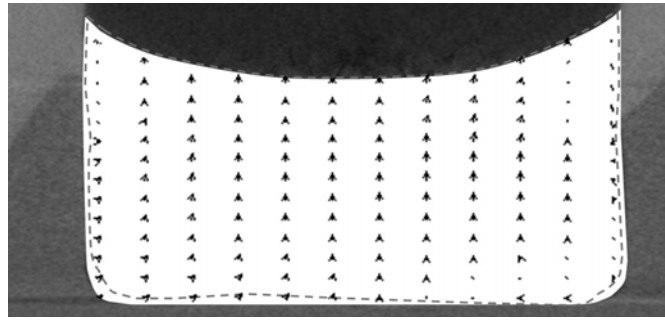
(B)
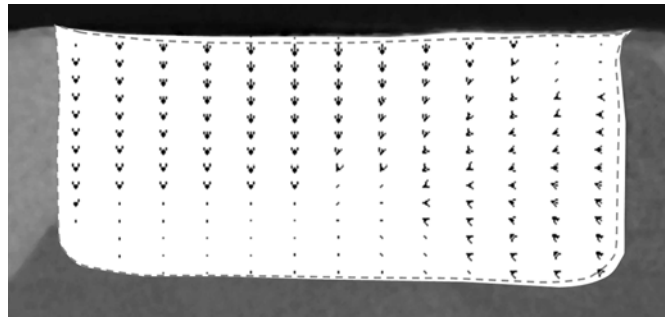
Figure 1-7. Shrinkage vectors distribution of bonded restorations.

(A) Bonded subgroup 1, slice along the xz-plane: The amount of enamel was similar along the margin of the cavity. The length of the vectors close to enamel is very small. In this example the displacement vectors point into the direction of the surface of the restoration. This can be explained with debonding at the bottom of the cavity.

(B) Bonded subgroup 2 (thicker enamel margin on the left side), slice along the xz-plane: The vector lengths at the right side close to the enamel interface are rather small. The vector length at the bottom of the cavity close to the long enamel interface is also rather small. Compensatory mass movement can be found close to the top of the restoration and on the right side at the dentin interface with the direction of the vectors pointing to the dentin attached composite at the left side of this slice. Debonding can be observed on the right side dentin wall.

Distribution Histograms of Vector Length Values
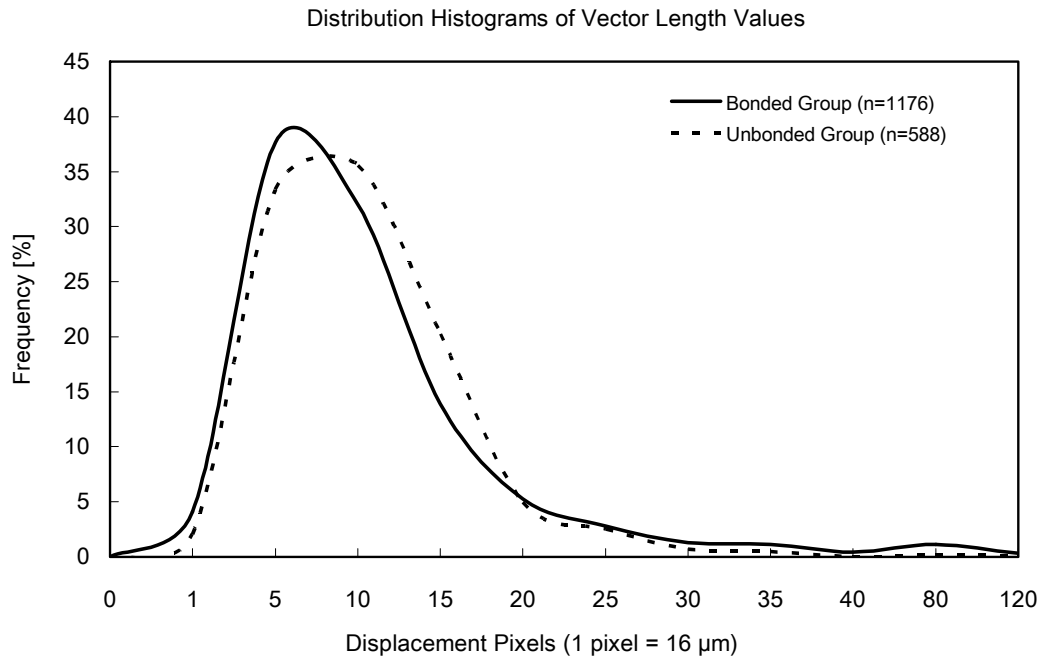
Figure 1-8. Histogram displaying deformation changes related to the vector length distribution (solid line: bonded group, n=1176; dotted line: unbonded group, n=588). The overall appearance of the two curves is quite similar. The primary maximum of the unbonded group represents smaller displacement values than the primary maximum of the bonded group. In addition, the bonded group exhibits a small secondary maximum, representing longer displacement vectors. This secondary maximum coincides with areas where debonding allowed more material displacement.

(A)
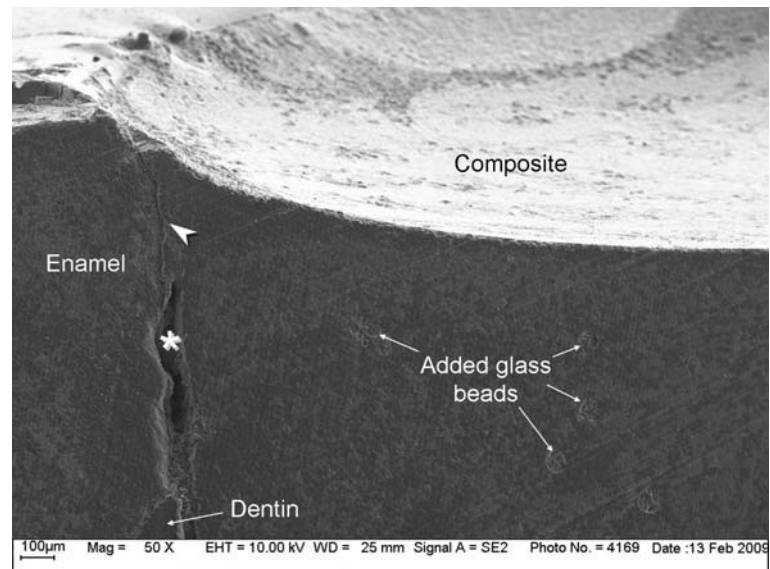
(B)
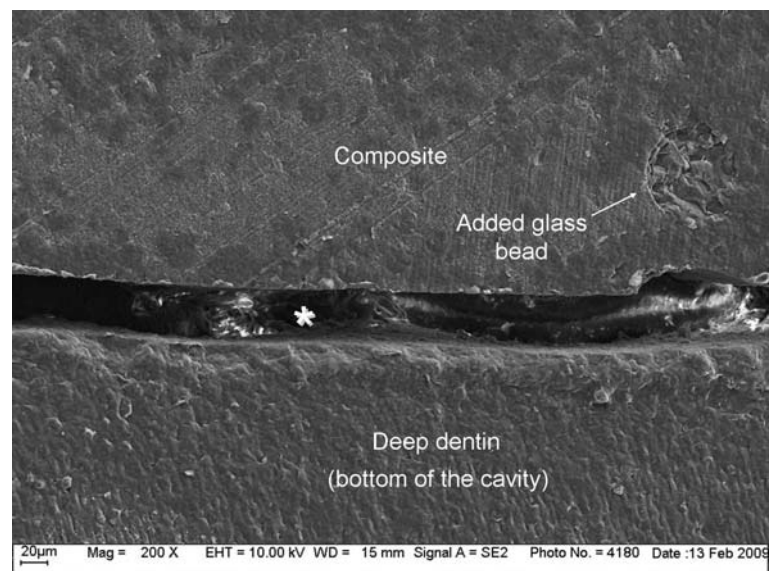
Figure 1-9. SEM examinations (bonded restoration, subgroup 1).

(A) The arrowhead pointed the adhesion adjacent to superficial enamel area create an optimal marginal adaptation. Beneath this area, the detachment was formed along the dentin-composite interface (star area). (B) Debonding at the bottom of the cavity (star area) allowed the composite material to move more toward the top surface. The silanized glass bead bonded well to the composite matrix (arrow).

(A)
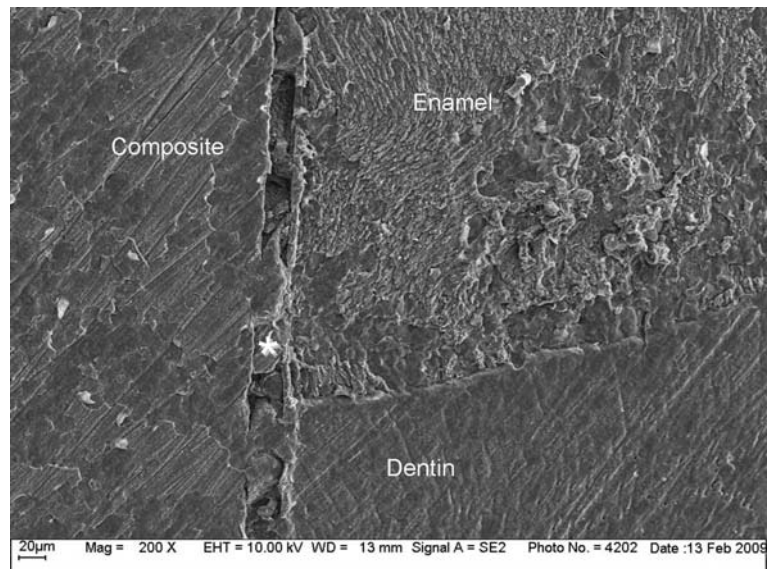
(B)
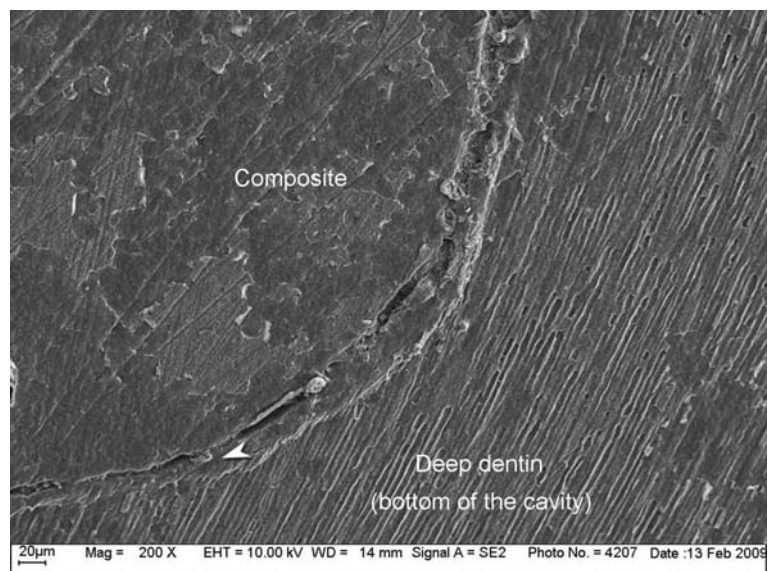
Figure 1-10. SEM examinations (bonded restoration, subgroup 2).

(A) A compensatory gap was formed at one side of the cavity (star area). (B) At the bottom of the cavity, the composite was in tight contact with dentin. The arrowhead indicated the hybridization from the adhesive and dentin substrate.

1.4 Discussion

Inai et al. (2002) first had the idea to trace radiopaque zirconium dioxide fillers with the use of a µCT. The zirconium dioxide fillers, however, introduce reconstruction artifacts to the µCT images and cannot establish a bond with the composite matrix, which might influence the resulting measurements due to stress relief around the fillers. We decided to use radiolucent glass fillers which were silanized to overcome both limitations. The greater shrinkage of the flowable resins was expected to help visualize the shrinkage vectors more easily. According to our study, 1.5 wt% of glass fillers is sufficient to provide the landmarks necessary to observe shrinkage. At the same time, polymerization of the flowable resin is scarcely affected.

The image registration algorithm used in this study is based on vector-spline regularization combined with B-spline based elastic registration (Kybic and Unser, 2003; Sorzano *et al.*, 2005). Image registration can be performed using both landmark-based and landmark-independent registration algorithms. During elastic registration, when the image exhibits major deformations or when the information is unevenly distributed, the landmark-based registration approach is superior to purely intensity-based registration algorithms. In our study, exaggerated local deformations sometimes appeared at the bottom of the cavity. The silanized glass filler "landmarks" were necessary in such a situation because without such landmarks, the underlying registration model would have masked these local effects.

In our control group, the displacement vector field (Fig. 1-6B) verifies the FEA findings that the photo-curing composites shrink towards the center under free

shrinkage conditions (Versluis *et al.*, 1998). However, the overall shrinkage direction is not towards the center of the restoration. The shrinkage direction is affected by the adhesion of the restoration to the tooth tissue. Even without the use of bonding agents, composite materials adhere to certain areas of the tooth surface, mediated for example by small surface irregularities. As soon as the contraction stress overcomes the weak initial adhesion to the tooth tissue, the restoration surface is detached from the weakest link first and shrinks, now essentially unimpeded, to the area which offers the most durable adhesion characteristics. This explains why the displacement vectors display an asymmetric shrinkage pattern (Fig. 1-6). The μCT evaluation method has a clear advantage over FEA in visualizing this asymmetry, because it is very complicated or even impossible to predict this observed detachment from the cavity wall using FEA.

For bonded restorations, the net mass movement followed two contraction patterns either to the top-surface of the restoration or to the bottom of the cavity. Where the overall movement direction pointed to the top-surface of the restoration, enamel thickness was equal along the cavity margin (Fig. 1-7A). The other subgroup exhibited only very thin enamel at one side of the cavity (Fig. 1-7B). This variation helped to explain our findings. Adhesion to the enamel remained intact while the bond to dentin was lost due to the contraction stress.

Only Fig. 1-7B was not consistent with this explanation. There was no gap formation (Fig. 1-10B) and the top-surface of the filling moved slightly downward, leading to larger vector lengths in this area. The bond to dentin that was proximal to enamel remained intact because the long enamel margin bore most of the load and protected the portion of the dentin bond that was closest to this area.

Based on our results, we can reevaluate the two dominant theories of mass movement during polymerization: shrinkage toward the center of mass and shrinkage toward the direction of the light. The results of our (unbonded) control group confirm the hypothesis of Versluis et al. (1998), namely that light-cured composites shrink toward the center of mass. In addition, Versluis et al. (1998) simulated a restoration with perfect bonding to enamel but absence of bonding to dentin. This case is similar to the subgroup of bonded teeth with enamel margins of equal thickness, where the bond to dentin at the bottom of the cavity failed (Fig. 1-7A and 1-9B). In the third simulation group studied by Versluis et al. (1998), researchers assumed a perfect bond to both enamel and dentin; this group may be partially correlated to subgroup 2 in our study (Fig. 1-7B) (with a thick enamel margin on one side and an intact bond at the bottom of the cavity, proximal to the area with a wide strip of enamel). In this case, the shrinkage was compensated for by the outer surface of the cavity, just as predicted by the FEA simulation.

In conclusion, the proposed method can visualize the real displacement vectors due to shrinkage. Utilizing this approach, it has the potential to re-evaluate and unify all current hypotheses concerning the magnitude and orientation of shrinkage vectors. It appears that, in this study, the bonding quality is a critical factor in evaluating the direction of polymerization contraction.

Chapter 2

3-D Deformation Analysis of Composite Polymerization Shrinkage from µCT Images

2.1 Background and Significance

Dimethacylate-based composites are always accompanied by a 1.5-6 % volumetric shrinkage when they are polymerized (Kleverlaan and Feilzer, 2005; Labella *et al.*, 1999) and even newly developed ring-opening monomers like the Siloranes still have a volumetric shrinkage of about 1 vol% (Weinmann *et al.*, 2005). The shrinking behavior of resin composites results from the formation of cross-linked polymeric chains out of monomers leading to bulk contraction and displacements within the curing material. The volume changes upon curing cause either marginal gaps or, in case of enduring adhesion, stress within the tooth or the restorative material.

In dental literature, controversial hypotheses state that light-cured resin-composites shrink toward the light source or, rather similar to self-cured resin-composites, shrink towards the center of mass (Asmussen and Peutzfeldt, 1999; Hansen, 1982a; Lutz *et al.*, 1986a). Based on this assumption, different techniques of resin composite application were proposed in order to improve the marginal integrity and reduce the contraction stress. Examples are light-reflecting wedges to improve the proximal marginal adaptation of Class II restorations (Lutz *et al.*, 1986b), the multiple increment technique (Liebenberg, 1996), and the modulation of the light intensity (Mehl *et al.*, 1997) or the use of low-modulus intermediate layers (Cunha *et al.*, 2006). However, there is little evidence regarding the direction of the polymerization

56

shrinkage vectors of light-initiated resin composite.

So far, only indirect methods, which usually evaluate the gap formation, are used to compare different composite-dentin bonding systems concerning their performance to obtain a tight marginal seal. These indirect methods have some inherent limitations. The dye penetration studies usually require the destruction of the samples by cutting to gain insight into deeper areas of the cavity. Sometimes, it is hard to differentiate whether the dye penetrates into a gap or stains the hydrophilic dentin bonding agent itself. Other methods, like the SEM analysis, can evaluate only superficial aspects. If native teeth are used, gaps due to drying artifacts cannot be differentiated from gaps due to shrinkage. If replica is made, then the quality of the replica limits the discriminative power of the SEM evaluation. The simulation of shrinkage based on FEA is another approach (Versluis *et al.*, 1998) but this approach usually does not allow predicting the behavior of a real material combination, because too many assumptions are necessary for the computer model.

In addition to the solo analysis of marginal gaps formation (Kakaboura *et al.*, 2007; Sun and Lin-Gibson, 2008), the µCT also offers the option to visualize changes between the situation before and after curing. Some investigators could even demonstrate that it is possible to follow individual fillers before and after curing and obtain information of the material flow inside a cavity due to polymerization (Inai et al. 2002). They used radiopaque zirconium dioxide fillers as tracer markers and further identified the individual fillers manually. Chiang et al. (2008) demonstrated that radiolucent glass beads can be used as tracer fillers, too. The glass beads have certain advantages. They can be silanized to establish a chemical bond to the composite matrix, which is necessary to avoid stress relief around unbonded fillers. In

addition to this, radiopaque fillers, like the zirconium dioxide fillers, introduce reconstruction artifacts in the µCT, which is not the case for the radiolucent glass fillers.

In Chapter 1, we have proposed an elastic registration algorithm using B-spline regulation to two-dimensionally visualize and analyze the contraction behavior of the composite material due to the light-initiated polymerization. To visualize the movement of the tracer markers, it is necessary to determine the positions of corresponding markers in both 3-D data sets. This should be done automatically to save time and avoid operator errors. Several methods exist to evaluate comparable problems in medical image analysis, like for example visualizing the volume change of tumors during treatment (Hajnal *et al.*, 2001).

The aim in this part of this study was (1) to develop a method to visualize the 3-D shrinkage vectors by experimentally analysing 3-D µCT data before and after curing light-initiated dental composites, and (2) to analyse the deformation changes of dental composites in different tooth-resin interface situation.

2.2 Materials and Methods

2.2.1 *Specimen preparation and experiment design*

The dimethacrylate based flowable resin composite (Tetric[®] EvoFlow, Ivoclar, Vivadent AG, Schann/Liechtenstein, Switzerland) was selected to obtain shrinkage values which can be clearly identified with the given μCT resolution. In order to visualize the material movement, radiolucent spherical glass fillers with an average particle size of 40-70 μm in diameter (Sigmund Linder GmbH, Warmensteinach, Germany), were chosen as traceable markers. As previous described (Chapter 1), the glass beads were silanized to ensure a durable connection to the composite. The total amount of glass beads added to the composite was approximately 1.5 wt%. A total of 6 intact molar teeth were selected and their cusp tips were removed to obtain a flat surface. The flat surface ensured a consistent and unimpeded access for light curing. A Class I tooth cavity, 3 mm in depth and 6 mm in diameter, was prepared. The Class I cavity was selected in order to eliminate as much elastic deformation of the tooth as possible and to comply with one of the models evaluated by Versluis et al. (1998). The teeth were divided into two groups. In the first group, the dentin surface was not pre-treated with a dentin bonding agent, while a self-etching dentin bonding agent was applied in the second group. The group without bonding served as a negative control. The tooth restored with the traceable resin composite was covered with a radiolucent, dark cap to avoid hardening of the resin composite during the μCT measurements. The restoration was digitized before and after light-curing (90 degree direction, 40 s, 950 mW/cm^2 light intensity, 8 mm light-tip diameter, LED SmartLight® PS, Dentsply/Caulk, DE, USA). The materials used in this study are described in Table 1-1 (Chapter 1).

2.2.2   X-ray micro-computed tomography measurement

A high resolution micro-computed tomography apparatus (µCT 40, Scanco Medical AG, Basserdorf, Switzerland) was used to evaluate the material movement due to the polymerization shrinkage of the light-curing composite. The settings for the µCT were: acceleration voltage 70 kVp and cathode current 114 µA. The samples were scanned with 8 µm resolution using an integration time of 600 ms and were never removed from the µCT attachment. Therefore, it was possible to directly compare the measurements before and after light-curing.

The 3-D data before and after polymerization were subjected to image segmentation and registration. The general idea of the whole process is to determine the center of the same spherical particle before curing and after curing and to describe the movement of the sphere as a displacement vector. The start point of the displacement vector is identical with the center of the sphere before curing while the end point of the displacement vector is identical with the center of the same sphere after curing.

2.2.3   Data processing

The deformation vector field is obtained in a three step approach. In the first step, the volume of the restoration is identified in the µCT data set (Fig. 2-1A). The subsequent evaluation is limited to this subimage only which will be called VOI (= volume of interest). The second step identifies the traceable markers and labels each marker individually in the VOI of the uncured composite (Fig. 2-1B). The last step determines the displacement vectors of the individual markers (Fig. 2-1C and 2-1D).

All displacement vectors are called the displacement vector field.

2.2.3.1   Subimage selection

Fig. 2-1A shows that the selection of the restoration volume is done interactively with the software InsightSNAP (www.itksnap.org). Restoration volumes selected from images acquired before and after curing are stored and used for subsequent image processing steps.

2.2.3.2   Sphere segmentation

This procedure identifies and separates the glass spheres from the rest of the restoration in the image taken before curing (Fig. 2-1B). As the gray value of the radiopaque glass spheres is smaller than that of the composite material, a threshold is applied to segment sphere candidates. Unique labels are assigned to each connected region that has been segmented. In order to restrict registration to spherical structures, the inertia tensor and its eigenvalues are determined for each labeled component. For ideal spheres, identical eigenvalues are expected so that regions for which the eigenvalues differ significantly are considered non-spherical and excluded from the remaining image processing steps.

2.2.3.3   Registration of individual spheres

Since the hardness of the glass beads significantly exceeds that of the composite, deformation of spheres during polymerization is not expected and a local rigid registration (block matching) can be performed to determine the displacement of segmented spheres during the polymerization process (Fig. 2-1C and 2-1D). This

block matching is described in detail in Rösch et al. (2009).

The overall outline of this process is like this. The largest sphere of the uncured situation is identified. Then, a spherical mask containing both the glass bead and some surrounding material in the uncured situation is determined. At the beginning of block matching, the coordinates of the sphere center are transferred to the cured situation and gray value cross correlation is optimized iteratively with respect to sphere displacement between cured and uncured situation. The calculation of cross correlation is restricted to the area corresponding to the spherical mask. One by one the displacement vector of each identifiable sphere is determined and stored. The combination of all individual displacement vectors is called the displacement vector field.

2.2.3.4   Deformation field visualization

Deformation field is visualized using VTK (www.vtk.org) version 5.0.4. The individual translation vectors are visualized starting from the midpoint of the selected sphere. For the printed figures, the length of the vectors is scaled with the factor 3 to enhance the visibility. The quantitative analysis of the vector length is performed with the unscaled vectors. The vector length (V_l) due to deformation is obtained as

$$V_l = \sqrt{x^2 + y^2 + z^2}$$

where *x, y and z* are components of the vector V in x, y and z direction. The total deformation change summarizes the overall amount of deformation independent of the direction of the deformation.

For a quantitative analysis, the length values of unscaled vectors were

summarized as a histogram. The mean and standard deviation (SD) of the histogram, the skewness and kurtosis were calculated to characterize the distribution of the deformation vector lengths.

2.3 Results

The segmentation and registration sequence is visualized in Fig. 2-1. In Fig. 2-2, Fig. 2-3, and Fig. 2-4, examples of the 3-D deformation vectors are shown as cone symbols. On the computer screen, the coordinate system can be rotated interactively in all directions. To make the orientation within the restoration easier, graylevel images of slices through the 3-D micro CT data can be projected into the vector coordinate system at any location within the bounding box.

Fig. 2-2 is an example for an unbonded; Fig. 2-3 and Fig. 2-4 are examples of bonded restorations. The cones represent both displacement vector length and orientation. In our case, the direction of the cones corresponds to the direction of the movement of the glass spheres while the length of the cones stands for the absolute sphere displacement. In the following, these two aspects are interpreted separately:

2.3.1   *Deformation field orientation*

In the unbonded control group, the composite usually adheres to one cavity side and is pulled from the other walls toward the adhering parts of the restoration (Fig. 2-2A and 2-2B). A compensatory gap is formed at the interface between the restoration and the tooth surface in non-adhering cavity areas.

For the bonded restoration group, two different outcomes can be observed and described as subgroups. In subgroup 1, by accident, the enamel at the cavity margins was thicker on one side of the cavity and thinner at those other parts. In this case, the predominant orientation of the displacement vectors field is toward the thicker enamel part of the cavity. The movement is not only toward the enamel margin, but also to the

underlying dentin parts of this direction (Fig. 2-3). At the vertical walls of the thin enamel margins, a radiolucent layer is frequently visible at the interface between the composite and the opposing dentin wall and can be interpreted as a gap formation. Those samples, which we classify as subgroup 2 had nearly the same enamel thickness around the whole cavity margin. The main orientation of the deformation vectors of subgroup 2 is usually towards the top-surface of the restoration (Fig. 2-4), while a radiolucent area was visible at the bottom of the cavity.

In general, the displacement vectors of the unbonded group are approximately but not perfectly oriented towards the center of the restoration (Fig. 2-2B) with an overall shift towards the adhering surface. In contrast to this, the direction of the displacement vectors of the bonded group depends on the subgroup and can direct toward the adhering part of the cavity (Fig. 2-3A) or toward the top surface of the restoration (Fig. 2-4A). In some cases, the level of the cured composite surface was even above the surface of the uncured composite.

2.3.2   *Statistical analysis of absolute local displacement*

The histogram of the distribution of all vector length values for each group/subgroup is shown in Fig. 2-5. The amount of mass movement depends on the adhesion to the cavity wall. The histogram can be described with the statistical parameters, mean (SD), skewness and kurtosis (Table 2-1). The main peak of the histogram in the bonded subgroup 1 (located at 40 μm) is similar with the main peak of the histogram in the unbonded group (located at 43 μm). In contrast to these two groups, subgroup 2 has two maxima. The main maximum is around 60 μm, while the secondary maximum is close to 30μm. The position of the secondary maximum

65

correlates with those parts of the restoration which exhibit little displacement, while the main maximum with a higher value represents parts of the restoration with more displacement of the glass spheres. The histogram curves can be further characterized with skewness and kurtosis. The unbonded group has a skewness of 0.3 and a kurtosis of 0.5. Subgroup 1 of the bonded group had a kurtosis of 35.2, which means that approximate 80 % of the vectors are within the range from 30 to 50 μm. In addition, the skewness of 3.6 means the histogram has a long tail to the right.

(A)
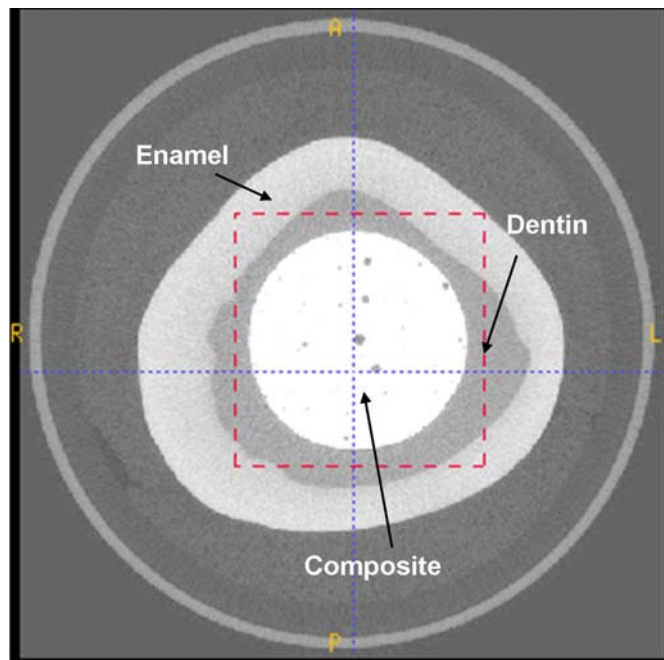
(B)
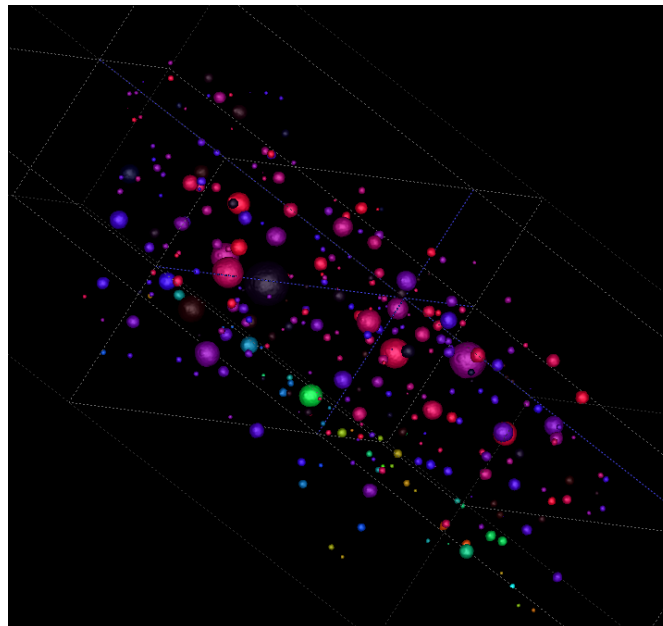
Figure 2-1. Workflow of the block-matching to determine the deformations vectors: (A) The region of interest is selected from the 3-D data stack of the µCT image. (B) The glass beads are segmented using a graylevel threshold followed by the exclusion of non-spherical objects. Each individual sphere is labeled.

(C)
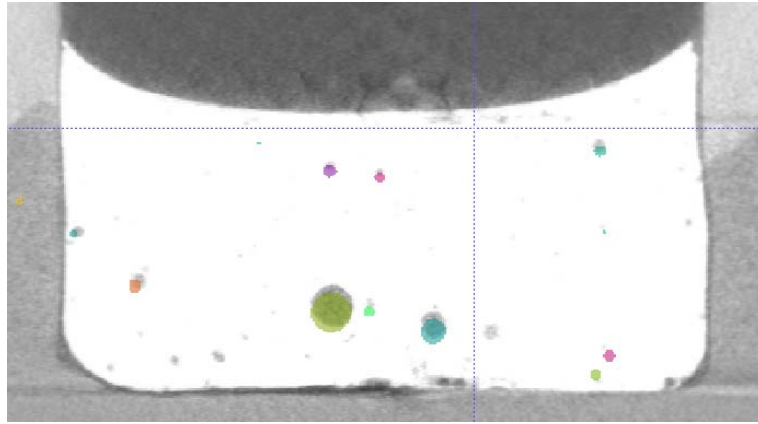
(D)
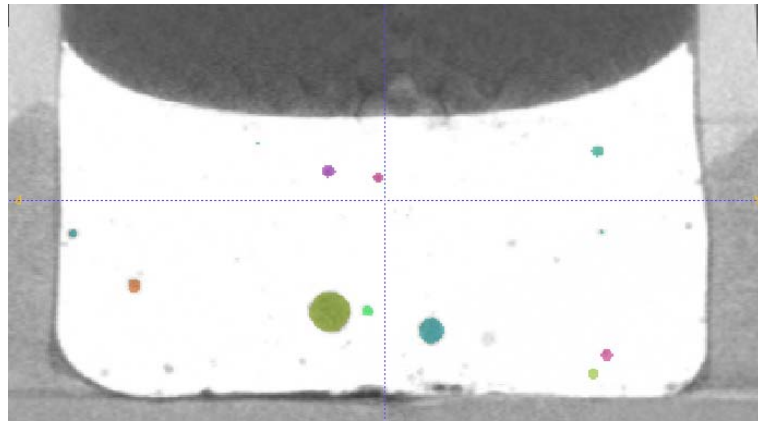
Figure 2-1. Workflow of the block-matching to determine the deformations vectors: Each individual sphere is labeled. The labels are color coded for visual control. (C) The segmented glass beads are superimposed to the corresponding gray value image after polymerization before and (D) after the block-matching registration.

(A)
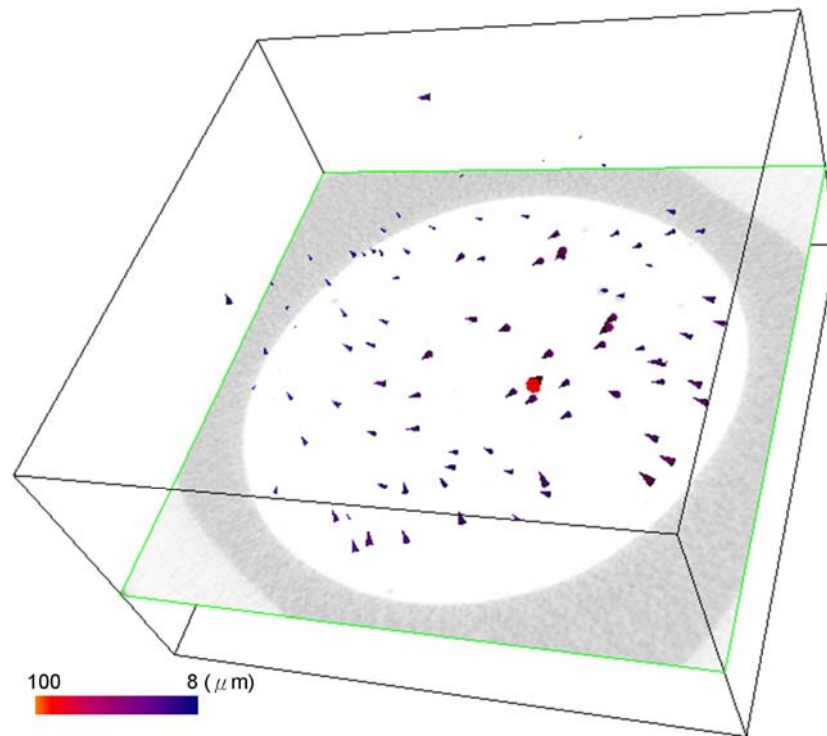
Figure 2-2. An example of the 3-D deformation vectors of the unbonded restoration. In addition to the visual vector representation, one graylevel image of a slice through the 3-D data stack is projected into the bounding box of the coordinate system to make it easier to correlate the vectors with the cavity. The images are rotated different so that the described effect can be seen most easily. (A) Horizontal view: Most vectors are oriented to the left side of this graph while the vector length is very small. A possible explanation for this finding is that the composite adheres to one side of the cavity even without bonding and as a consequence the compensatory mass movement due to shrinkage is into the direction of this attachment to the cavity wall.

(B)
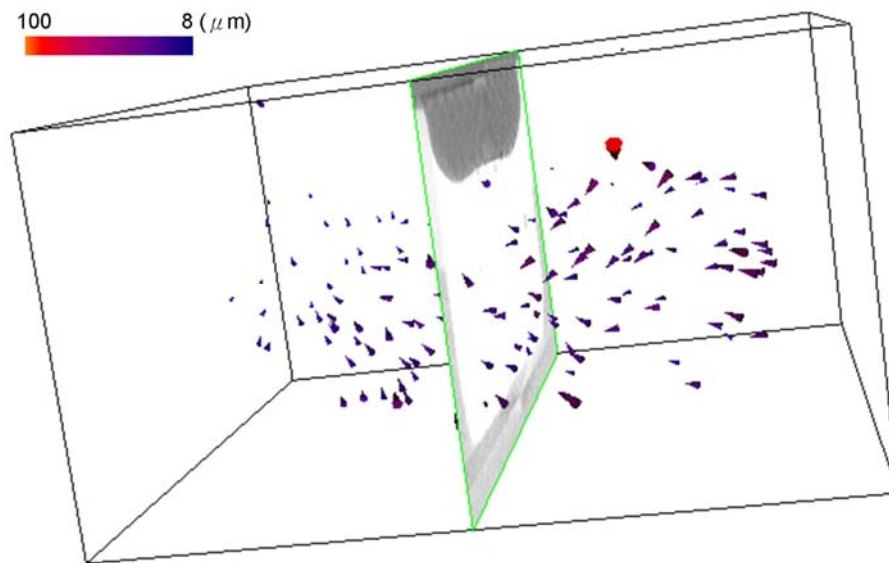
Figure 2-2. An example of the 3-D deformation vectors of the unbonded restoration. (B) Side-view: From the side-view we can see a wave-like vector flow within the cavity which causes a slight inflection of the surface of the restoration after curing. The vectors are represented by color-coded cones. The base of the cone is identical with the start point of the vector, while the tip of the cone is the end point of the vector where cones have been scaled by a factor of three to enhance visibility. The color code is added as a legend to the figures.

(A)
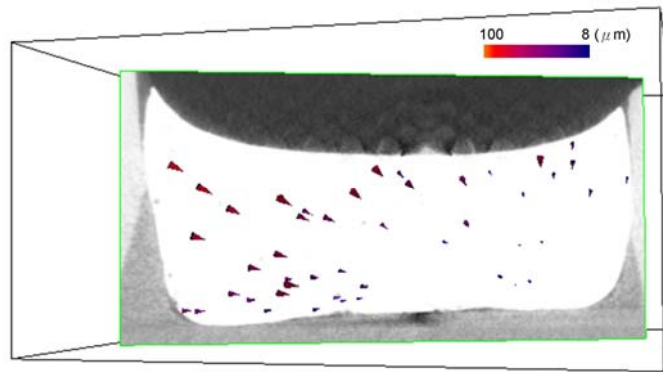
(B)
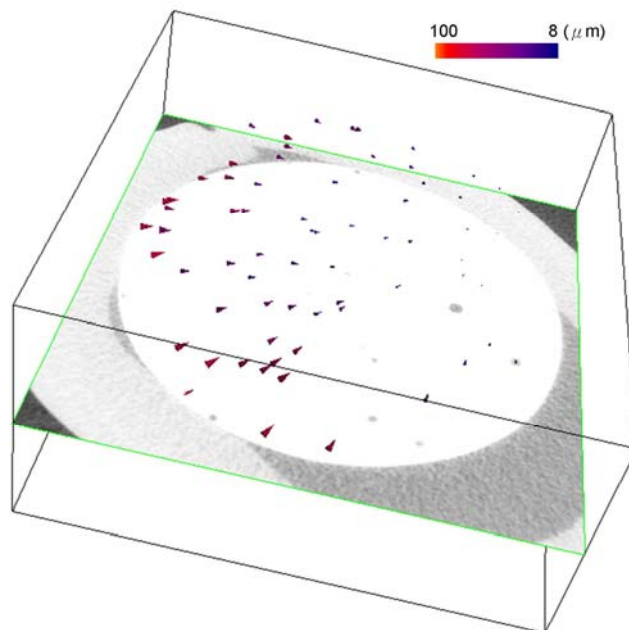
Figure 2-3. An example of the 3-D deformation field of bonded restoration which is defined as subgroup 1 (unequal enamel thickness along the margin of the cavity). The images are rotated different so that the described effect can be seen most easily. (A) The shrinkage vectors are directed toward the bottom of the cavity at the side where the enamel margin is thicker (right-hand side). The vector length at the bottom of the cavity close to the long enamel interface is rather small. (B) Again we find a compensatory mass movement near the top of the restoration and on the left side interface pointing toward the attached composite on the right side of this cavity. Note that cones have been scaled by a factor of three to enhance visibility.

(A)
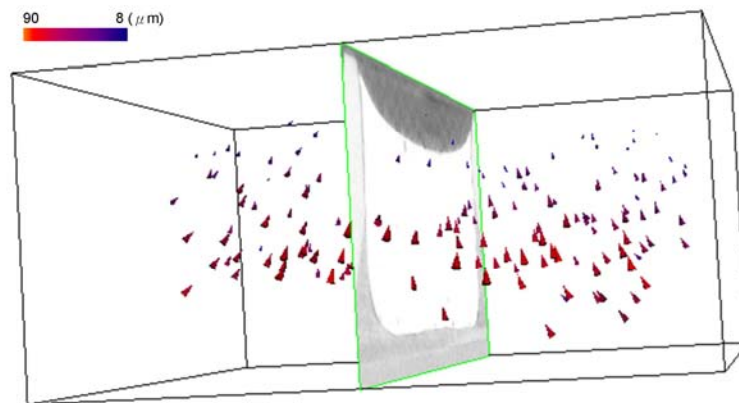
(B)
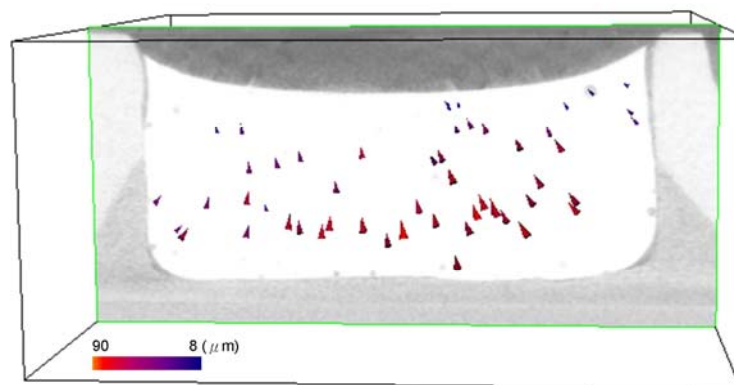
Figure 2-4. An example of the 3-D deformation field of bonded restoration defined as subgroup 2 (equal enamel thickness along the margin of the cavity). The images are rotated different so that the described effect can be seen most easily. Note that cones have been scaled by a factor of three to enhance visibility.

(A) Close to the enamel margin, the vector lengths are rather short. In general, the displacement vectors point toward the surface of restoration. (B) Debonding can be observed at the bottom of the cavity.
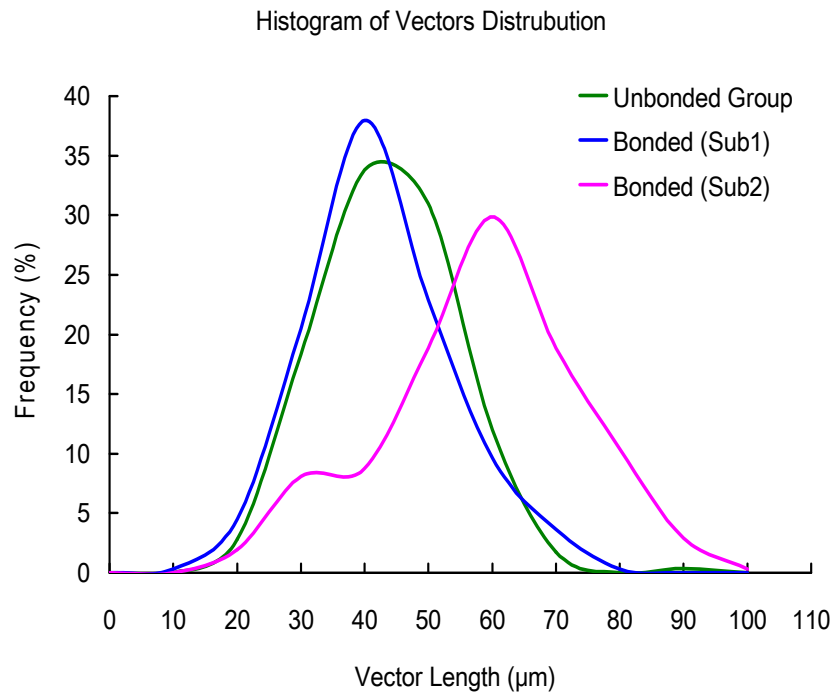
Figure 2-5. Histogram of the vector length distribution (green line: unbonded group; blue line: bonded subgroup 1; pink line: bonded subgroup 2).

The overall appearance of the "unbonded group" and the "bonded subgroup 1" curves is similar. The main maximum of the "unbonded group" and the "bonded subgroup 1" represents smaller displacement values than the main maximum of the "bonded subgroup 2". In addition to the main maximum (~ 60 μm), the "bonded subgroup 2" has a second maximum representing shorter displacement vectors (~ 30 μm). This second maximum coincides with areas close to enamel, where the material exhibits less displacement.

Table 2-1. Statistical Parameters of the Histograms

	N	Mean (SD) [μm]	Skewness	Kurtosis
Unbonded group	284	38.7 (10.6)	0.3	0.5
Bonded (subgroup 1)	332	37.8 (13.6)	3.6	35.2
Bonded (subgroup 2)	308	53.4 (15.5)	- 0.3	-0.02

2.4 Discussion

The displacement of each glass bead in general originates from two independent processes: The motion of the entire sample due to repositioning that can be described by a global 3-D rigid transformation (i. e. translation and rotation) and the motion of each individual sphere relative to the cavity walls originating from polymerization shrinkage. As the sample was not removed from the micro CT device for curing and visual inspection of overlay images clearly indicated that the sample sample position was not changed during the procedure, global rigid registration is not required and only the second process needs to be corrected for by non-rigid registration.

For the non-rigid registration, several alternative algorithms are available (Hajnal *et al.*, 2001). Chiang et al. (2008) used an elastic spline-based registration for the 2-D analysis of the same shrinkage problem. The idea of the elastic registration in 2-D is to distort a regular grid by moving some points of the grid to a new position. The grid itself is elastic and it costs energy to deform the grid. Larger deformations require more energy. The overall goal of the elastic registration is to fit the grid to the new position by using as little energy as possible. The points where the grid is deformed are identical to the tracer markers. The regular grid is applied to the situation before polymerization, while the deformed grid represents the situation after curing. According to the optimization function the deformed grit is close to the fillers after curing, but due to the energy criterion, the grid lines will not be identical to the position of the fillers after curing.

Rösch et al. (2002) developed an alternative method based on block matching. A simplified version of this approach was used in the present study (Rösch *et al.*, 2009).

For the given application, it can be safely assumed that the displacement of the largest spheres is smaller than their radius. Thus, image regions corresponding to the largest fillers in the cured and uncured situation overlap. Experimental results show that this overlap is sufficient to allow for an accurate iterative gray value based registration of these objects. As no disruptions of the composite during polymerization have been observed, continuous deformation fields with similar displacement vectors for neighboring spheres can be expected. It follows that the displacement of the large spheres can be used to predict the displacement of adjacent smaller fillers. The predicted translation vectors were used as starting estimates which where further refined by applying the same iterative local rigid registration procedure that had been used for the larger spheres. Fillers which could not be registered accurately were excluded from the analysis.

Block matching guarantees that each identifiable filler pair before and after curing is exactly represented by a displacement vector. This makes it superior to the spline-based elastic registration. The only disadvantage of block matching might be that the displacement vector density depends on the distribution of the tracer markers in the composites. In our case, some datasets exhibited an uneven filler distribution. This is due to the fact that the fillers were mixed by hand into the flowable composite. But this can be easily improved with mechanical mixers. Our current study was intended as a proof of concept and to develop the method. The uneven filler distribution does not influence the results or the interpretation of the results. It is just a cosmetic disadvantage of the graphs and can be easily compensated for in future experiments.

In our study, we decided to compare to extreme situations, composite

restorations without any adhesive and composite restorations with a self-etching dentin bonding. Both groups were also evaluated with FEA simulations by Versluis et al. (1998). The FEA simulation of the unbonded group of light curing composites exhibited a rather uniform shrinkage toward the center of mass of the restoration (Versluis *et al.*, 1998). Our result does not coincide with the FEA simulation (Versluis *et al.*, 1998), but this does not necessarily mean that our results are different. The shrinkage direction is affected by the adhesion of the filling material to the tooth tissue, especially the enamel margin on the left side of the graph in Fig. 2-2. Even without using dentin bonding agents, resin composites can adhere to certain areas of the cavity surface probably due to mechanical surface irregularities. At the beginning, the adhesion to the cavity wall is statistically distributed. Consequentially, once the contraction stress overcomes the weakest attachment to the tooth tissue, the restoration surface is detached from this area and shrinks now nearly unimpeded to the area which offers the most durable adhesion. The displacement vectors therefore display an asymmetric shrinkage pattern (Fig. 2-2A).

To visualize this asymmetry, it is a clear advantage of the μCT evaluation method over the standard FEA where uniform boundary conditions are assumed. However, combining the μCT results with advanced FEA including comparable boundary conditions should reveal similar results. Thus, it would be possible to identify complex boundary conditions with the μCT analysis and vary material parameters easily with the FEA.

The results of the bonded restorations are at the first glance totally different from the results predicted with FEA. Even within this group, we found two different shrinkage patterns: in subgroup 1, we observed an overall direction of the deformation

vector towards one side of the cavity, and in subgroup 2, the general direction was oriented towards the surface of the restoration. The interpretation of this finding is not intuitive in the beginning. But the detailed analysis of the 3-D graylevel images revealed an interesting difference between the two groups. The thickness of the enamel along the margin of the restorations was not uniform in all samples. In fact, the samples of subgroup 1, where the direction of the movement vectors was oriented to one side of the cavity, exhibited asymmetrical enamel thickness along the cavity margin (Fig. 2-3A). This variation was not intended, initially, but could not be overcome due to the biological variation of the substrate. However, this variation provided interesting insight into the consequences of adhesion variations within a cavity. Dentin bonding agents may exhibit higher bond strength to cut enamel than to dentin (Goracci *et al.*, 2004). Reflecting the displacement vectors based on this premise, the movement of the tracer particles should be less close to enamel limited areas when compared to dentin limited parts of the cavity. This also helps to understand our findings. The wider enamel margin provides better adhesion than the narrower enamel margins of the cavity. Therefore, the curing contraction causes debonding at the narrow enamel margins with a much higher probability than at the wide enamel margins, because the long enamel margin probably withstands the contraction stress, carries most of the load and therefore protects the dentin bond close to this area. As soon as the restoration detaches from one side of the cavity, the remaining adhesion is protected because now the composite nearly behaves like in the unbonded situation: it shrinks towards the intact bonding areas. As a consequence, the dentin bond below a wide enamel margin is preserved longer than the dentin bond at the opposite side, where detachment is initiated.

In those cases, where the overall shrinkage vectors are oriented to the top of the restoration surface (subgroup 2), the enamel thickness was equal along the cavity margin (Fig. 2-4B). The displacement field presented in these cases is similar to the FEA study that assumed that the restoration is perfectly bonded to enamel only (Versluis *et al.*, 1998). In this FEA simulation model, the shrinkage vectors were oriented upwards within the dentin part because the composite detached from the unbonded bottom of the cavity.

While the surface of the restoration in the FEA model was slightly lower after curing, the restorations surface in subgroup 2 was slightly higher and therefore outside of the original shape. This variation between the FEA model and the real restoration in Fig. 2-3 and 2-4 can be interpreted by the different shape of the restorations surfaces. The composite surface in the FEA model was a linear connection between the opposing margins. In Fig. 2-3 and 2-4, the surface shape is concave. This means that the enamel margins are slightly above the central part of the surface of the restoration. The enamel thickness was evenly distributed along the margin. The adhesion to enamel stays intact while the bond to dentin is lost due to the contraction stress. As soon as the bond to dentin is lost, the stresses are relieved and the tracer particles move towards the areas inside the cavity where the bond is preserved. After the restoration is detached from the dentin, it is slightly pulled upwards by the contraction stress, too.

The observations which we described here for the dentin bonding agent Prompt L-Pop might be totally different for other dentin bonding agents. This example, however, nicely shows the potential for a detailed evaluation of the 3-D data with the µCT.

In addition to the qualitative analysis, the vector length data provide a quantitative measure to compare the different groups. For example, we formulated the hypothesis that the unbonded group and subgroup 1 of the bonded samples behave similar. This hypothesis is confirmed when be compared the histogram curves of the two groups. The mean of the main maximum is nearly identical and the small difference between the two means in combination with the standard deviation support this hypothesis. It would be necessary, however, to increase the sample size for an appropriate statistical proof.

The difference between subgroup 1 and 2 for the bonded group is also confirmed by their histograms. In this case, the differing main maxima as well as the shapes of the histograms curves justify the separation into the subgroups. The absolute values of the main maxima of the unbonded group and the subgroup 1 of the bonded group are plausible, too, if one assumes a linear shrinkages of 1 % for the composite material in a 6 mm wide cavity.

Another example of a nice advantage of the non-destructive 3-D analysis with the μCT is the validation of the nature of the radiolucent areas at the interface between the restoration and the cavity walls. For example, in Fig. 2-4B, one cannot say whether the radiolucent area is a marginal gap or a visible layer of radiolucent dentin bonding agent. The availability of the 3-D data before curing makes it easy to differentiate between a gap and a thick layer of dentin bonding agent. In case of Fig. 2-4B, we could confirm that the radiolucent layer corresponds to the dentin bonding agent. As a side effect, this evaluation also shows how difficult it is to obtain a uniform layer of dentin bond throughout the whole cavity.

Last but not least, we would like to point out that when Lutz et al. (1986a) claimed that the shrinkage vectors are oriented toward the light source, the observation, which leads to this conclusion, was correct. However, we should reevaluate their observations with the μCT analysis, which we presented in this study. In addition to their original setup, we should vary the cavity boundary conditions, too. It might be that the results leading to their claim were influenced more by the boundary conditions, as already formulated (Asmussen and Jorgensen, 1972), than the direction of light.

Chapter 3

Evaluation of Dentin Bonding Agents Effects on Composite Polymerization Shrinkage Using 3-D Registration from μCT Images

3.1 Background and Significance

The volume shrinkage of composite restorations upon curing either cause marginal gaps, or stress within the tooth and the restoration. The competition between the contraction stress of resin composite and bond strength to tooth cavity affects the mass movement. Despite significant improvements of adhesive systems, the bonded interface does remain the weakest area of tooth-composite restorations. With the increasing number of new adhesives, often introduced to the market without sufficient documentation of their clinical effectiveness, interpretation of in vitro data as possible predictors for usefulness remains a difficult challenge. Post-cure cavity adaptation or microleakage, which has been identified as the main problem in dentistry with respect to polymerization shrinkage (Ferracane, 2008; Lutz *et al.*, 1986a), is correlated with stress levels and the tooth-composite interfacial bond strength.

Optimal adaptation is required for adhesion; consequently, these movements may be detrimental to the infiltration of the substrate (Feilzer *et al.*, 1990). For optimizing marginal adaptation, different techniques of resin composite application were proposed in order to improve the marginal integrity and reduce the contraction stress (Ciamponi *et al.*, 1994; Giachetti *et al.*, 2006; Lutz *et al.*, 1986b). Regulation of the direction of polymerization shrinkage and microleakage represents a challenge for composite restorations. However, the resin composite materials would not know in

82

which direction to shrink. Our developed method can visualize the real polymerization shrinkage vectors orientation via 2-D and 3-D image registrations. For the bonded composite restoration, the disruption of the composite-dentin bond allows the material to move toward the composite-enamel bond (Chapter 1, Fig. 1-7A and 1-9). Based on the results of Chapter 2 and Chapter 3, we know the bonding quality (adhesion hybrid layer) is crucial to determine the direction and amount of polymerization shrinkage.

In the current study, self-etch adhesives are combined with resin composite materials, differing in polymerization contraction and stress, and evaluated with regard to bonding strengths and marginal adaptation in standardized butt-joint dentin cavities. Bond strength data only give very little information in this respect, whereas cavity adaptation or microleakage evaluations together with 3-D shrinkage vectors within tooth-restoration may offer more insight to acknowledge the use of self-etch dentin bonding agents (Chiang *et al.*, 2008; Sun and Lin-Gibson, 2008). In particular, interactions between different adhesives and resin composites are rarely recognized.

In this part of the study, we try to evaluate the effects of different self-etching dentin bonding agents on the polymerization shrinkage behavior of a light-initiated composite within the dentin cavity using 3-D μCT datasets combined with the developed images registration strategy as described in Chapter 2. The approach of high resolution X-ray micro-computed tomography (μCT) using cone-beam geometry is currently able to exhibit true 3-D images of the structure of small samples. In order to obtain the test cavity with fully-dentin wall, we try to make a smaller and uniform dentin cavity to diminish the influences by the regional difference of tooth structure.

3.2 Materials and Methods

Non-carious human permanent molars were collected and stored in distilled water containing 0.2% thymol at 4˚C. The flat dentin surface was exposed by cutting perpendicular to the long axis of the tooth using a precision diamond saw under water cooling. All sectioned teeth were examined under the stereo optical microscope to ensure no remaining enamel.

3.2.1 Tooth cavity preparation

Class I trapezoidal cylindrical cavities (d1 x h x d2 = 4mm x 2.5mm x 2.5mm) were prepared and then embedded in the μCT sample holder (Fig. 3-1 and 3-2). Three self-etch bonding agents, XenoV (Dentsply, Konstanz, Germany), Clearfil-SE-Bond (Kuraray, Okayama, Japan) and OptiBond (Kerr, CA, USA) were tested for this study. The compositions of DBAs used in this study are listed in the Table 3-1. The application of DBAs was performed according to the instruction of manufacturers. The cavity geometry in this part of the study is smaller than our previous studies. Therefore, in order to be easily recognized and traced from μCT images, we increase the ratio of traceable glass beads in light-initiated resin composite (Tetric Flow) up to 5 wt% (Chapter 1, Table 1-1).

3.2.2 X-ray micro-computed tomography

The procedure of the specimen preparation was as previously described (Chapter 2 and 3). The cavity was filled with traceable resin composite (Fig. 3-2B) and the restoration was digitized before and after light-curing (40 s, 950 mW/cm^2 light intensity, 8 mm light-tip diameter, LED SmartLight$^®$ PS, Dentsply/Caulk, DE, USA)

with a micro-computed tomography apparatus (μCT 40, Scanco Medical AG, Basserdorf, Switzerland).

The settings for the μCT were: acceleration voltage 70 kVp and cathode current 114 μA. The samples were scanned with 16 μm resolution using an integration time of 300 ms and were never removed from the μCT attachment. The obtained 3-D data before and after polymerization were subjected to an image analysis.

3.2.3 Images analysis and registration

As previous described (Chapter 2), image segmentation was performed to extract these glass beads from the acquired 3-D μCT images (uncured and cured) and then subjected to registration based on a block matching algorithm. The resulting 3-D displacement vector fields were used to examine the polymerization shrinkage vectors distribution.

For a quantitative comparison, the vector length values were summarized as a histogram. The mean and standard deviation (SD) of the histogram, the skewness and kurtosis were calculated to characterize the distribution of the deformation vectors.
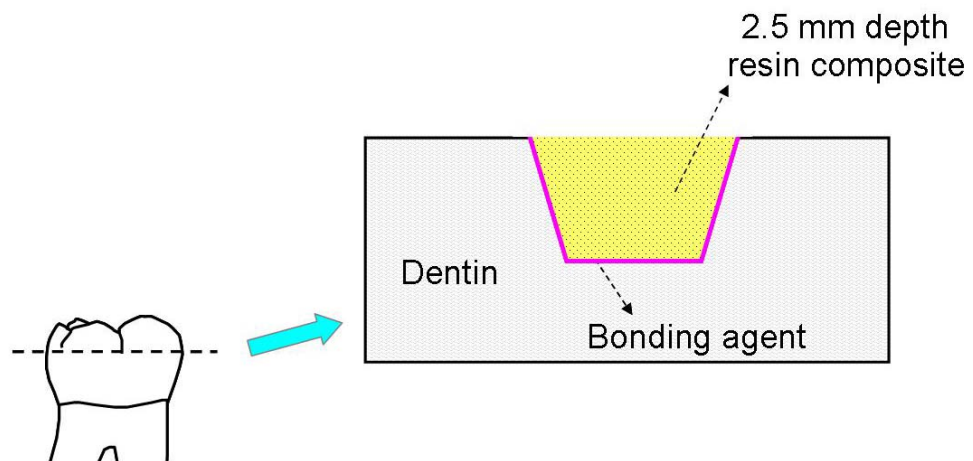
Figure 3-1. Schematic representation of trapezoidal cylindrical cavity preparation
and resin composite restoration. d1= upper diameter of cavity, h=height of cavity,
and d2= lower diameter of cavity.

(A)

(B)

Figure 3-2. Sample preparation for μCT measurement. (A) Class I tooth cavity preparation. (B) The embedded tooth was applied with self-etch adhesive and filled with the traceable resin composite.

Table 3-1. Composition of Self-Etch Adhesives Used in this Study

Adhesives	Composition	Batch No.	Manufacturer
Clearfil SE Bond	Primer: 2-hydroxyethyl methacrylate 10-30%, Other ingredients: 10-methacryloyloxydecyl, dihydrogen phosphate, hydrophilic aliphatic dimethacrylate, dl-camphorquinone, water, accelerators, dyes, others Bond: Bisphenol A diglycidylmethacrylate 25-45%, 2-hydroxyethyl methacrylate 20-40%, Other ingredients: 10-Methacryloyloxydecyl, dihydrogen phosphate, hydrophobic aliphatic dimethacrylate, colloidal silica, dl-Camphorquinone, initiators, accelerators, others	LOT: 01106A	Kuraray Medical Inc. 1621 Sakazu, Kurashiki, Okayama, 710-0801, Japan
OptiBond	Acetone 35-45%, ethyl alcohol 4-9%, uncured methacrylate ester monomer 33-43%, Other ingredients: Inert mineral fillers, ytterbium fluoride, photo-initiators, accelerators, stabilizers and water	LOT: 3101942	Kerr Corporation. 1717 West Collins Avenue, Orange, CA, 92867-5422, USA
XenoV	Bifunctional acrylates 25-50%, acrylic acid 2.5-10%, tert-butyl alcohol 2.5-10%, functionalized phosphoric acid ester 2.5-10%, acidic acrylate $\leq$ 2.5%, phosphine oxide photoinitiator $\leq$ 2.5%	LOT: 0801000603	DENTSPLY DeTrey GmbH. De-Trey-Str. 1, D-78467, Konstanz, Germany

3.3 Results

The corresponding radiolucent glass beads, which added to the resin composite, can be recognized and extracted from the 3-D datasets of μCT images. Again, the displacement vectors field after the block matching method can be displayed in VTK (www.vtk.org) and clearly showed the displacement of the glass beads after curing (Fig. 3-3, 3-4 and 3-5). For the printed figures, the length of the vectors is scaled with the factor 8. The quantitative analysis of the vector length is performed with the unscaled vectors.

Two polymerization contraction patterns were exhibited in this study: either toward the bottom of the cavity (Clearfil SE Bond and OptiBond adhesives) shown in Fig. 3-3A and Fig. 3-4A or toward the top-surface of the restoration (XenoV adhesive) shown in Fig. 3-5A. The main maximum the histogram of XenoV adhesive bonded restoration (Fig. 3-5B, skewness/kurtosis: 0.7/0.3) and OptiBond (Fig. 3-4B, skewness/kurtosis: 0.5/-0.7) restorations represent larger displacement value (located at 30 μm) than the main maximum of the Clearfil SE Bond adhesive bonded restoration, which located at 20 μm (Fig. 3-3B, skewness/kurtosis: 0.5/0.5). In addition to the main maximum, the XenoV adhesive bonded restoration has 2 minor peaks which represented the shorter (located at about 12 μm) and the longer (located at about 50 μm) displacement vectors, respectively. The shorter vectors coincide with areas close to coronal dentin where the material exhibits less displacement.

(A)
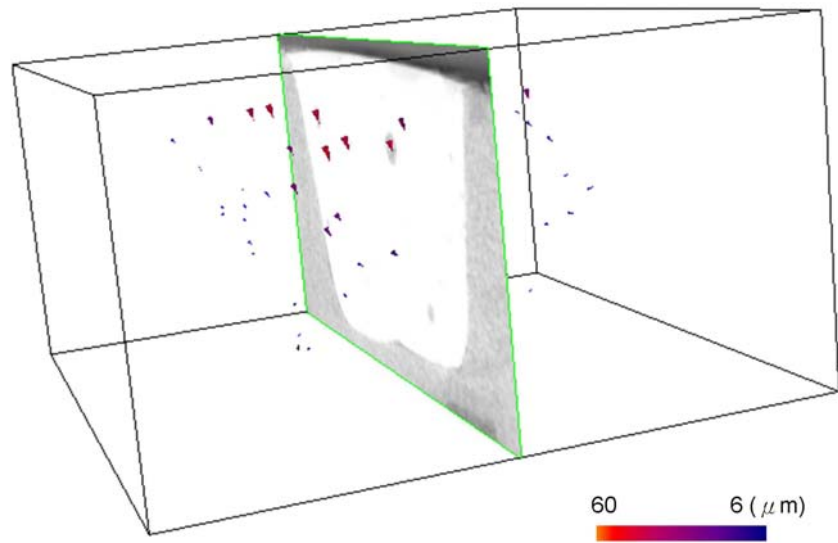
(B)
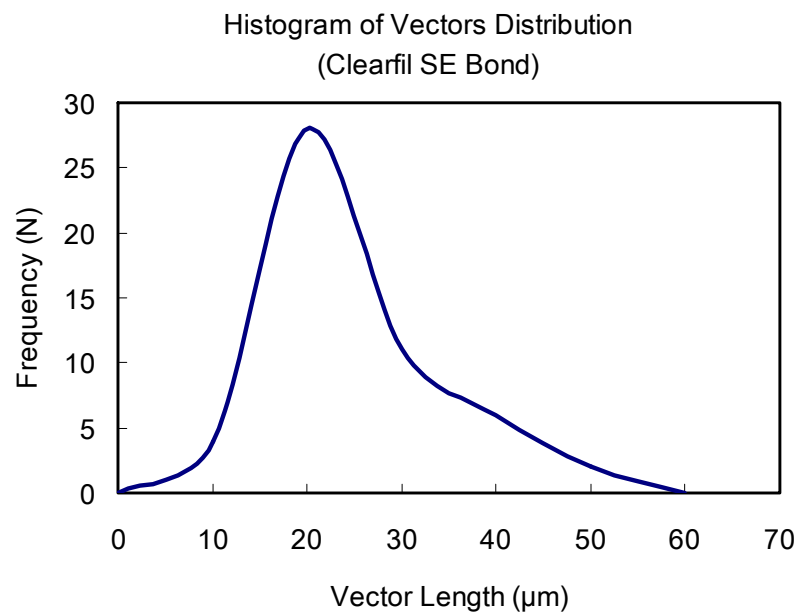
Figure 3-3. (A) 3-D displacement vector field of Clearfile SE Bond adhesive bonded restoration. The cones represent the displacement vectors with a scale factor 8. (B) Histogram of unscaled vector lengths distribution.

(A)
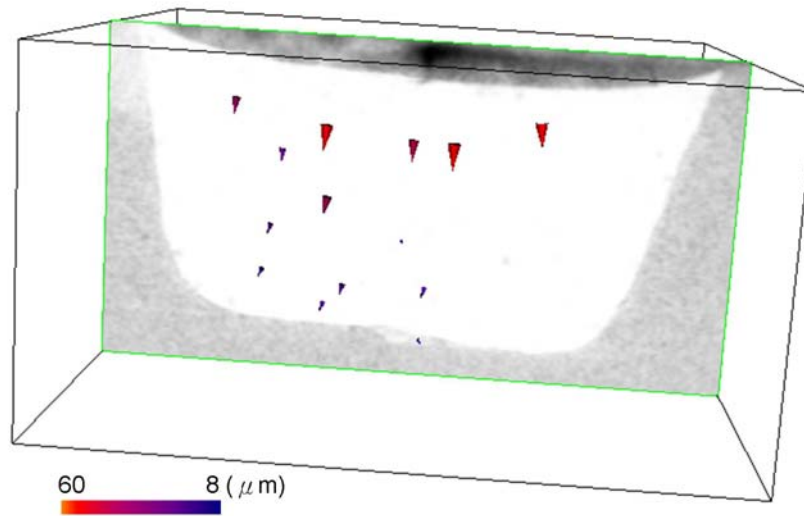
(B)
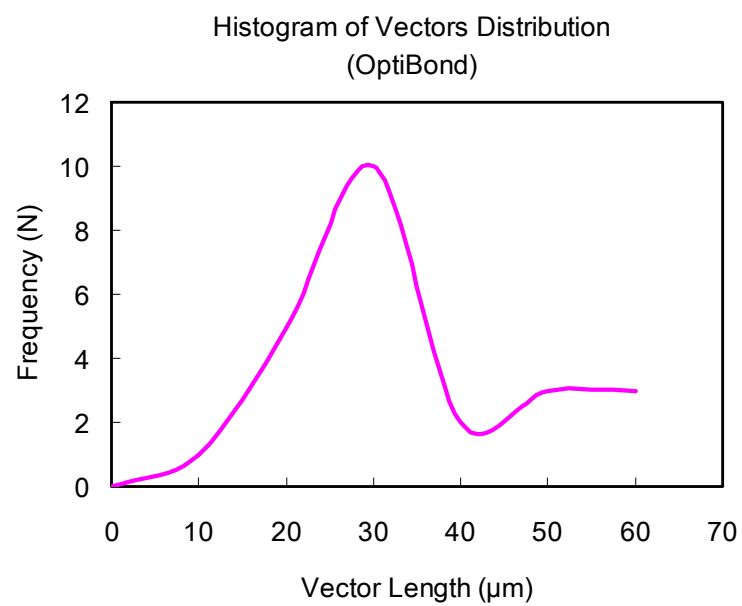
Figure 3-4. (A) 3-D displacement vector field of OptiBond adhesive bonded restoration. The cones represent the displacement vectors with a scale factor 8. (B) Histogram of unscaled vector lengths distribution.

(A)
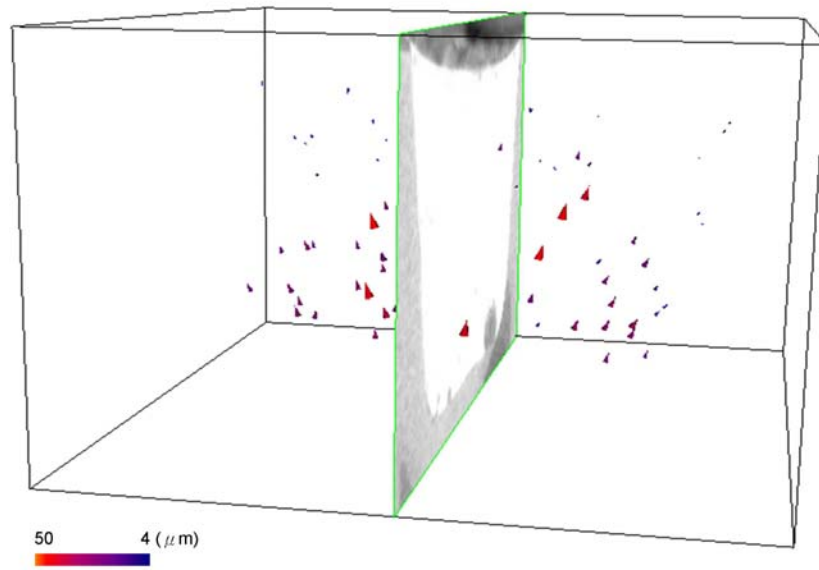
(B)
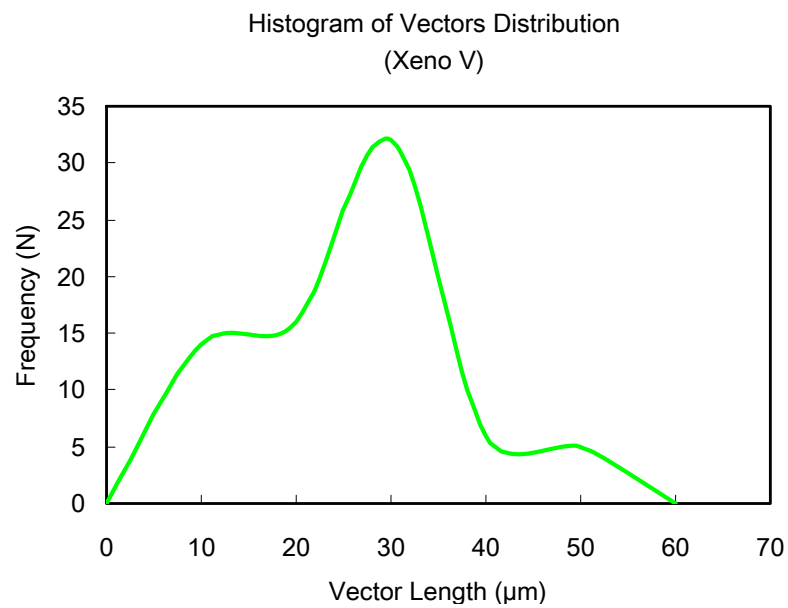
Figure 3-5. (A) 3-D displacement vector field of XenoV adhesive bonded restoration. The cones represent the displacement vectors with a scale factor 8. (B) Histogram of unscaled vector lengths distribution.

3.4 Discussion

A number of new dentin bonding systems have been developed in an attempt to obtain a reliable bond to dentin and further changed the philosophies of cavity preparation. In order to reach a reliable hybridization (bonding quality) and save operation time, the self-etch adhesive systems are currently used. The self-etch primers, for example the Clearfil SE Bond (two-steps) adhesive system, are to combine the acid and primer in one solution to form an acidic monomer and then a final step of bonding is applied (Nakabayashi and Pashley, 1998). Another approach is the use of one-step self-etch systems, for example OptiBond and XenoV adhesives, which bonding mechanism is based on the simultaneous etching, priming and bonding to the smeared dental hard tissue with only one single solution (Tay and Pashley, 2001).

For a composite material, it is inevitable that residual stresses will exist within the material when undergoes polymerization shrinkage. It is also inevitable that some of this stress will be delivered to the surrounding bonded interfaces (Feilzer *et al.*, 1987; Ferracane, 2008; Giachetti *et al.*, 2006). Thus, the interactions, the direction of shrinkage vectors, between the composite material and the adhesion (dentin bonding agent) should be acknowledged. In order to create a uniform boundary condition, we removed the enamel portion and unified tooth cavities in this study. That is to say that we have the same volume of the filling material, the same cavity geometry, and similar dentine substrate. The shrinkage behavior is mainly controlled by the boundary conditions, i.e., the shape of the cavity and the features of the margins, which include bonded as well as free surfaces. In OptiBond adhesive bonded cavity (Fig. 3-4A), some larger vectors near the free surface (top surface) of restoration are

93

oriented downward to compensate for the materials contraction due to polymerization. If we examine its histogram distribution, a secondary maximum located at 50-60 μm represents the longer vectors near the top surface were oriented toward the bottom of the cavity. However, for the Clearfil SE Bond adhesive bonded cavity (Fig. 3-3A), which its histogram showed a normal distribution (skewness/kurtosis: 0.5/0.5) and no secondary maximum (longer vectors), the 3-D μCT image represented that somewhere along the cavity walls existed marginal gaps after the polymerization. Consequently, the resulting marginal gaps may not only cause esthetic problems but allow bacteria (plaque) to accumulate and propagate during the cycling thermal changes and the occlusal load.

It seems an advantage for optimizing the marginal seal if the materials shift toward the bottom and lateral walls despite of the bond strength value. Certainly, the consequence of movement causes the larger shrinkage vectors formation from the free surface toward the bottom of the cavity. However, if the shrinkage vectors pointed toward the top surface of the restoration, for example XenoV adhesive bonded cavity in this study (Fig. 3-5), the adhesion at the bottom of the cavity would be lost due to the polymerization shrinkage. Therefore, even though the coronal marginal seal is intact after the polymerization, the stressed or weak bonded interfaces between the dentin wall and composite material may be broken (debonded) due to the cyclic loading from occlusal function. Though the enamel portion was removed in this study, the bonding quality can be affected by the regional differences of the dentin substrate, i.e. the wetness and the orientation of dentinal tubules. The diameter of the dentinal tubules decreases from 2.5 μm near the pulp side (deep dentin) to 0.8 μm near the dentin-enamel junction (superficial dentin). Moreover, the number of the dentinal

94

tubules decreases from about 45000/mm^2 near the pulp to about 20000/mm^2 near the dentin-enamel junction (Garberoglio and Brannstrom, 1976). In general, the deep dentin which exits larger diameter of tubule and less collagen fibers would result in lower bonding strength and unreliable bonding quality when compare to the superficial dentin (Pereira *et al.*, 1999; Proenca *et al.*, 2007). Bond strengths of more recent self-etching adhesive systems (one-step or two-step self-etch approach) that modify the smear layer and partially dissolved smear plugs and therefore, diminishing the sensitivity to the regional variability of dentin structure (Pereira *et al.*, 1999; Summitt *et al.*, 2006).

It is interesting to note that the direction of shrinkages vectors in XenoV adhesive bonded restoration was divergently oriented from the bottom of the cavity toward the top surface and lateral walls (Fig. 3-5A). In general, the nature of the contraction pattern in light-cured composite materials has a tendency which always shrinkage toward the center of the mass even if in a bonded cavity. Is it a finding in conflict with the results of our previous studies (Chapter 1 and 2)? We would say that the cavity geometry (divergent shape) influenced the direction of the shrinkage vectors. Therefore, the bond strengths between the lateral dentin walls and the composite material are strong enough to pull the material up and toward the later dentin walls. The certain amount of extreme values (Fig. 3-5B) in the histogram of XenoV adhesive bonded restoration, i.e. the peak of shorter vectors (~10 μm) coincide with the area close to superficial lateral dentin walls in which the composite material exhibits less displacement, at the same time, the peak of larger vectors (~50 μm) represented a larger movement of the composite material near the bottom of the cavity (deep dentin). This can be correlated with the finding of Lutz et al. (1986a) that

marginal adaptation can be improved when a composite restoration was light-cured at the margin. This effect has been widely attributed to shrinkage vectors of the composite material being oriented toward these margins. However, this is only one of the observations; again, we would not say that the materials shrink toward the light but the rational explanation should base on our results: the dominant influences in the shrinkage vectors of the light-initiated composite can be the cavity geometry the bonding quality which is changed due to regional differences of dentin substrate or the properties of adhesives.

In conclusion, it is clear that our proposed 3-D block match images registration method can be applied to analyze small tooth cavities and evaluate the adhesion of different DBAs to dentin substrate. According to the above statements and our findings, we can make a comment that XenoV adhesive is more sensitive to the bonded dentinal substrate, whereas Clearfil SE Bond and OptiBond adhesives may appear to be less affected by the regional differences of the dentin substrate. Moreover, the composite materials can move to any area in which the interfacial adhesion is predominant. In other words, the DBA system should be chosen according to the dental regional substrate and cavity geometry to be bonded, since bond strengths can vary according to the wetness, geometry, and the adhesive system.

Summary Statement

The introduction to this dissertation summarized the main tasks of the work into two major hypotheses:

(1) The polymerization shrinkage vectors could be visualized by the registration of corresponding markers in µCT images, which were recorded before and after curing.

It is ascertained that the suggested method can visualizes the real deformation vectors due to curing contraction. With the 3-D registration method, the real deformation vectors of restorations within different DBAs bonded cavity due to curing contraction can be visualized as well. The examples which we demonstrated clearly show that the bonding quality at the interface restoration-tooth is a very critical factor in evaluating the direction of polymerization contraction.

(2) Light-curing dental composites do not always shrink toward the light.

For the given situation, this hypothesis must be accepted as true. However, with regard to the findings of Lutz et al. (1986a), we would argue that they reported accurate observations, but their explanations for these findings have to be reappraised based on our new findings. Instead of explaining their observations in terms of shrinkage toward the direction of light, perhaps these findings should be better explained as suggested by Versluis et al. (1998), with a simulation that is limited to the enamel bond. Instead of assuming no bond at all for the dentin surface, we included a weak bonding agent in our experiments.

The results suggest that we should no longer discuss the duality of these theories but rather a synthesis of both, the nature of which is determined by the bonding conditions to the different tooth tissues. We would speculate that a third hypothesis should be integrated for a comprehensive understanding of displacement due to curing contraction: the influence of the configuration of the cavity as it is formulated by the hypothesis of the configuration factor (Feilzer *et al.*, 1987).

In summary, the qualitative and quantitative analysis of the vector field in combination with the grayvalue data supply more insight into the shrinkage behavior of adhesive-restoration-systems in real teeth with all their variations of the boundary conditions than with any currently available method. Therefore, this new approach has the potential to reevaluate and hopefully unify all the currently available hypotheses concerning the length and orientation of shrinkage vectors.

Zusammenfassung

Die Gruppe der dentalen Komposite stellt eine wichtige Werkstoffkategorie in der zahnmedizinischen Füllungstherapie dar. Physikalisch und chemisch bedingt weisen Komposite nach der Polymerisation eine Volumenabnahme auf, die zu Randspalten beziehungsweise Spannungen am Übergang zwischen Zahn und Füllungen führen kann. Zahnärzte versuchen, die Folgen der Kontraktionsschrumpfung auszugleichen, indem sie das Material in unterschiedlichen Schichten auftragen und die einzelnen Schichten individuell aushärten. Im Zusammenhang mit der Richtung der Schrumpfungsvektoren gibt es zwei widersprüchliche Hypothesen. Zum einen wird postuliert, dass die Komposite in Richtung Lichtquelle schrumpfen (Lutz et al. 1986). Dem steht die Alternativhypothese gegenüber, dass die Komposite immer zu Massemittelpunkt hin kontrahieren (Versluis et al. 1998). Bisher war es nicht möglich, die Schrumpfungsvektoren zu visualisieren, um diese Frage eindeutig zu klären. Im Rahmen der vorliegenden Dissertation sollte daher versucht werden, die Länge und Richtung der Schrumpfungsvektoren zu visualisieren.

Anhand von physikalischen und chemischen Vorüberlegungen wurden als Ausgangsbasis zwei Hypothesen formuliert:

(1) Die Folgen der Polymerisationsschrumpfung können durch die Registrierung von Referenzmarken in µCT Bilder, die vor und nach der Aushärtung aufgenommen werden, visualisiert werden.

(2) Die lichthärtenden Komposite schrumpfen nicht immer zur Lichtquelle hin.

Die Folgen der Polymerisationsschrumpfung wurden visualisiert, indem

Glaskugeln in Modell-Komposite gemischt wurden. Die Menge der Glaskugel war mit circa einem Gewichtsprozent relativ gering. Darüber hinaus waren die Glaskugeln mit Silan vorbehandelt, so dass davon ausgegangen werden kann, dass der Einfluss der Glaskugel auf die Polymerisationsschrumpfung zu vernachlässigen ist. Die Glaskugeln können mithilfe von hochauflösenden Microcomputertomographie- aufnahmen visualisiert werden. Um die Vektoren für die Polymerisationsschrumpfung zu bestimmen, mussten vor und nach Polymerisation korrespondierende Kugeln identifiziert werden.

Die Verschiebevektoren wurden zunächst zweidimensional, später drei- dimensional bestimmt. Bei der zweidimensionalen Visualisierung wurden die Prüfkörper mechanisch exakt positioniert und die Verschiebung der Glaskugeln in der gleichen Schicht mithilfe eines elastischen Registrierungsalgorithmus nach der Vektor-Spline-Regularisierung bestimmt. Diese Methode kann als Vorversuche betrachtet werden, in dem geklärt werden sollte, ob die Auflösung des µCT zur Beantwortung der Fragestellung ausreichend ist oder nicht. Da diese Fragestellung positiv beantwortet werden konnte, wurde in Kooperation mit dem Lehrstuhl für Informatik der Fachhochschule Augsburg (Prof. Rösch) eine dreidimensionale Methode entwickelt, die nach der Methode des „Block-Matching" arbeitet.

Die zweidimensionale und dreidimensionale Auswertung bestätigten Hypothese (1), dass es möglich ist, mithilfe von µCT-Aufnahmen, geeigneten Modellkompositen und Bildverarbeitungsalgorithmen Schrumpfungsvektoren zu visualisieren.

Um Hypothese (2) zu überprüfen, wurden Füllungen ohne Dentinadhäsiv und mit Dentinadhäsiv verarbeitet. Der Verzicht auf die Anwendung eines Dentinadhäsivs

sollte die Frage klären, ob die Komposite zum Massenmittelpunkt oder zu Lichtquelle hin schrumpfen. Er stellte sich heraus, dass die Komposite ohne Dentinadhäsiv im Prinzip zum Massemittelpunkt hin schrumpfen. Da jedoch aufgrund von mikromechanischen Verankerungen eine gewisse Restaffinität zu einer Seitenwand der Kavität erhalten war, bewegt sich die gesamte Füllung insgesamt in Richtung dieser Wand. Durch den Einsatz eines Dentinadhäsivs wurden die Schrumpfungsvektoren dahingehend beeinflusst, dass eine Teilmenge der mit Dentinadhäsiv vorbehandelten Füllungen ein ähnliches Verhalten aufwies, wie die unbehandelten Proben. Dies kann man so erklären, dass der Verbund zwischen Zahnhartsubstanz und Komposit in dem Moment gelöst wird, in dem die Polymerisationskontraktion die Haftung zum Zahn überschreitet. Die zweite Teilmenge unterschied sich von der ersten dadurch, dass die Schrumpfungsvektoren nicht zu einer Kavitätenwand hin, sondern zur Oberseite der Füllung orientiert worden. Diese beiden Teilmengen entsprachen im Wesentlichen den beiden in der Literatur genannten antithetischen Hypothesen. Dank der hochauflösenden µCT Aufnahmen war es möglich, eine weitergehende Analyse durchzuführen. Es zeigte sich nämlich, dass sowohl die Geometrie der Kavität als auch die Qualität der Restzahnhartsubstanz eine entscheidende Rolle für die Schrumpfungsvektoren spielen. In der Gruppe, die in Richtung Füllungsoberfläche schrumpfte, blieb der Verbund im Bereich der Füllungsränder nahezu vollständig intakt. Dies hing primär davon ab, wie die Schmelzranddicke um den Kavitätenrand verteilt war. Bei einer homogenen Schmelzdicke löste sich die Füllungen meist am Kavitäten Boden ab. Bei einer inhomogenen Schmelzdicke löste sich die Füllungen in der Regel an der Stelle ab, die der größten Schmelzdicke gegenüber lag.

Die genaue Analyse dieser Ergebnisse deutet darauf hin, dass sowohl die Hypothesen von Lutz et al. (1986a) als auch von Versluis et al. (1998) zu treffen. Die Aussagen von Versluis treffen vor allem dann zu, wenn keine Interaktion zwischen Komposit und Zahnhartsubstanz festgestellt werden kann. Die Aussagen von Lutz lassen sich mit homogenen Randbedingungen am besten erklären.

Wir sollten somit nicht mehr über die Dualität dieser Theorien, sondern eher über eine Synthese der beiden diskutieren, wobei der Natur der Verbindung zu den verschiedenen Zahngeweben eine entscheidende Rolle zugemessen werden muss.

Zusammenfassend ist festzustellen, dass die qualitativen und quantitativen Analyse der Vektorfeld in Kombination mit der Grauwert-Daten neue Einblicke in das Verhalten der Schrumpfung der Klebstoff-Füllmaterial-Systeme in realen Zähnen mit allen ihren Variationen der Randbedingungen liefern als mit jedem derzeit verfügbaren Methode. Daher hat diese neue Vorgehensweise das Potenzial, alle derzeit verfügbaren Hypothesen über die Ausrichtung der Polymerisations-schrumpfung zu neu bewerten und hoffentlich vereinheitlichen. Die Ergebnisse zeigen auch, dass idealisierte FEM-Simulationen derzeit noch stark vereinfacht sind und die klinische Realität nicht wiedergeben können.

REFERENCES

Alomari Q, Ajlouni R, Omar R (2007). Managing the polymerization shrinkage of resin composite restorations: a review. *Sadj* 62(1):12, 14, 16 passim.

Anseth KS, Goodner MD, Reil MA, Kannurpatti AR, Newman SM, Bowman CN (1996). The influence of comonomer composition on dimethacrylate resin properties for dental composites. *J Dent Res* 75(8):1607-12.

Arganda-Carreras I, Sorzano COS, Marabini R, Carazo JM, C. O-d-S, J. K (2006). Consistent and elastic registration of histological sections using vector-spline regularization. *Lect Notes Comput Sci* 4241:85-95.

Asmussen E, Jorgensen KD (1972). A microscopic investigation of the adaptation of some plastic filling materials to dental cavity walls. *Acta Odontol Scand* 30(1):3-21.

Asmussen E, Peutzfeldt A (1998). Influence of UEDMA BisGMA and TEGDMA on selected mechanical properties of experimental resin composites. *Dent Mater* 14(1):51-6.

Asmussen E, Peutzfeldt A (1999). Direction of shrinkage of light-curing resin composites. *Acta Odontol Scand* 57(6):310-5.

Asmussen E, Peutzfeldt A (2001). Influence of pulse-delay curing on softening of polymer structures. *J Dent Res* 80(6):1570-3.

Atai M, Watts DC (2006). A new kinetic model for the photopolymerization shrinkage-strain of dental composites and resin-monomers. *Dent Mater* 22(8):785-91.

Barnes DM, Thompson VP, Blank LW, McDonald NJ (1993). Microleakage of Class 5 composite resin restorations: a comparison between in vivo and in vitro. *Oper Dent* 18(6):237-45.

Barron DJ, Rueggeberg FA, Schuster GS (1992). A comparison of monomer conversion and inorganic filler content in visible light-cured denture resins. *Dent Mater* 8(4):274-7.

Bernardo M, Luis H, Martin MD, Leroux BG, Rue T, Leitao J, DeRouen TA (2007). Survival and reasons for failure of amalgam versus composite posterior restorations placed in a randomized clinical trial. *J Am Dent Assoc* 138(6):775-83.

Bichacho N (1994). The centripetal build-up for composite resin posterior restorations. *Pract Periodontics Aesthet Dent* 6(3):17-23; quiz 24.

Bouillaguet S, Gamba J, Forchelet J, Krejci I, Wataha JC (2006). Dynamics of composite polymerization mediates the development of cuspal strain. *Dent Mater* 22(10):896-902.

Bouschlicher MR, Rueggeberg FA, Boyer DB (2000). Effect of stepped light intensity on polymerization force and conversion in a photoactivated composite. *J Esthet Dent* 12(1):23-32.

Bowen RL (1963). Properties of a silica-reinforced polymer for dental restorations. *J Am Dent Assoc* 66:57-64.

Braga RR, Ferracane JL (2002). Contraction stress related to degree of conversion and reaction kinetics. *J Dent Res* 81(2):114-8.

Cabrera E, de la Macorra JC (2007). Polymerization shrinkage influences microtensile bond strength. *J Dent Res* 86(3):227-31.

Camps J, Dejou J, Remusat M, About I (2000). Factors influencing pulpal response to cavity restorations. *Dent Mater* 16(6):432-40.

Chan DC, Browning WD, Frazier KB, Brackett MG (2008). Clinical evaluation of the soft-start (pulse-delay) polymerization technique in Class I and II composite restorations. *Oper Dent* 33(3):265-71.

Chen HY, Manhart J, Hickel R, Kunzelmann KH (2001). Polymerization contraction stress in light-cured packable composite resins. *Dent Mater* 17(3):253-9.

Chen TM, Brauer GM (1982). Solvent effects on bonding organo-silane to silica surfaces. *J Dent Res* 61(12):1439-43.

Chiang YC, Rösch P, Lin CP, Hickel R, Kunzelmann KH (2008). Deformation Analysis of Composite Polymerization Shrinkage from μCT Images. Annual Meeting of the Academy of Dental Materials, October, Wurzburg, Germany.

Cho BH, Dickens SH, Bae JH, Chang CG, Son HH, Um CM (2002). Effect of interfacial bond quality on the direction of polymerization shrinkage flow in resin composite restorations. *Oper Dent* 27(3):297-304.

Chowdhury NA, Wakasa K, Priyawan R, Yamaki M (1997). Dental application of binary urethane monomer mixtures:strengthened resin matrix. *J Mater Sci Mater Med* 8(3):149-55.

Ciamponi AL, Del Portillo Lujan VA, Ferreira Santos JF (1994). Effectiveness of reflective wedges on the polymerization of composite resins. *Quintessence Int* 25(9):599-602.

Clementino-Luedemann TN, Dabanoglu A, Ilie N, Hickel R, Kunzelmann KH (2006). Micro-computed tomographic evaluation of a new enzyme solution for caries removal in deciduous teeth. *Dent Mater J* 25(4):675-83.

Condon JR, Ferracane JL (1998). Reduction of composite contraction stress through non-bonded microfiller particles. *Dent Mater* 14(4):256-60.

Craig RG (2006). Restorative Dental Materials. 12th ed.: Mosby.

Cunha LG, Alonso RC, Sobrinho LC, Sinhoreti MA (2006). Effect of resin liners and photoactivation methods on the shrinkage stress of a resin composite. *J Esthet Restor Dent* 18(1):29-36; discussion 36-7.

Dauvillier BS, Aarnts MP, Feilzer AJ (2000). Developments in shrinkage control of adhesive restoratives. *J Esthet Dent* 12(6):291-9.

Davidson CL, de Gee AJ (1984). Relaxation of polymerization contraction stresses by flow in dental composites. *J Dent Res* 63(2):146-8.

Davidson CL, de Gee AJ, Feilzer A (1984). The competition between the composite-dentin bond strength and the polymerization contraction stress. *J Dent Res*

63(12):1396-9.

Davidson CL (1986). Resisting the curing contraction with adhesive composites. *J Prosthet Dent* 55(4):446-7.

Davidson CL, Van Zeghbroeck L, Feilzer AJ (1991). Destructive stresses in adhesive luting cements. *J Dent Res* 70(5):880-2.

Davidson CL, Feilzer AJ (1997). Polymerization shrinkage and polymerization shrinkage stress in polymer-based restoratives. *J Dent* 25(6):435-40.

de Gee AF, Feilzer AJ, Davidson CL (1993). True linear polymerization shrinkage of unfilled resins and composites determined with a linometer. *Dent Mater* 9(1):11-4.

de Gee AJ, Davidson CL, Smith A (1981). A modified dilatometer for continuous recording of volumetric polymerization shrinkage of composite restorative materials. *J Dent* 9(1):36-42.

De Santis R, Mollica F, Prisco D, Rengo S, Ambrosio L, Nicolais L (2005). A 3D analysis of mechanically stressed dentin-adhesive-composite interfaces using X-ray micro-CT. *Biomaterials* 26(3):257-70.

Deligeorgi V, Mjor IA, Wilson NH (2001). An overview of reasons for the placement and replacement of restorations. *Prim Dent Care* 8(1):5-11.

Dewaele M, Asmussen E, Devaux J, Leloup G (2006). Class II restorations: influence of a liner with rubbery qualities on the occurrence and size of cervical gaps. *Eur J Oral Sci* 114(6):535-41.

Dietschi D, Marret N, Krejci I (2003). Comparative efficiency of plasma and halogen light sources on composite micro-hardness in different curing conditions. *Dent Mater* 19(6):493-500.

Eick JD, Kotha SP, Chappelow CC, Kilway KV, Giese GJ, Glaros AG, Pinzino CS (2007). Properties of silorane-based dental resins and composites containing a stress-reducing monomer. *Dent Mater* 23(8):1011-7.

Ernst CP, Kurschner R, Rippin G, Willershausen B (2000). Stress reduction in resin-based composites cured with a two-step light-curing unit. *Am J Dent* 13(2):69-72.

Feilzer A (1989). Polymerization shrinkage stress in dental composite resin restorations-an in vitro investigation [thesis]. *Amsterdam, The Netherlands: University of Amsterdam (ACTA)*.

Feilzer AJ, De Gee AJ, Davidson CL (1987). Setting stress in composite resin in relation to configuration of the restoration. *J Dent Res* 66(11):1636-9.

Feilzer AJ, de Gee AJ, Davidson CL (1990). Relaxation of polymerization contraction shear stress by hygroscopic expansion. *J Dent Res* 69(1):36-9.

Feilzer AJ, Dooren LH, de Gee AJ, Davidson CL (1995). Influence of light intensity on polymerization shrinkage and integrity of restoration-cavity interface. *Eur J Oral Sci* 103(5):322-6.

Ferracane JL, Marker VA (1992). Solvent degradation and reduced fracture toughness in aged composites. *J Dent Res* 71(1):13-9.

Ferracane JL (2008). Buonocore Lecture. Placing dental composites--a stressful experience. *Oper Dent* 33(3):247-57.

Friedl KH, Schmalz G, Hiller KA, Markl A (2000). Marginal adaption of Class V restorations with and without "softstart-polymerization". *Oper Dent* 25(1):26-32.

Gallo JR, Burgess JO, Ripps AH, Walker RS, Winkler MM, Mercante DE, Davidson JM (2005). Two-year clinical evaluation of a posterior resin composite using a fourth- and fifth-generation bonding agent. *Oper Dent* 30(3):290-6.

Garberoglio R, Brannstrom M (1976). Scanning electron microscopic investigation of human dentinal tubules. *Arch Oral Biol* 21(6):355-62.

Giachetti L, Scaminaci Russo D, Bambi C, Grandini R (2006). A review of polymerization shrinkage stress: current techniques for posterior direct resin restorations. *J Contemp Dent Pract* 7(4):79-88.

Goncalves F, Pfeifer CS, Ferracane JL, Braga RR (2008). Contraction stress determinants in dimethacrylate composites. *J Dent Res* 87(4):367-71.

Goracci C, Sadek FT, Monticelli F, Cardoso PE, Ferrari M (2004). Microtensile bond strength of self-etching adhesives to enamel and dentin. *J Adhes Dent* 6(4):313-8.

Hajnal JV, Hill DLG, Hawkes DJ (2001). Medical Image Registration. London: CRC Press.

Hansen EK (1982a). Visible light-cured composite resins: polymerization contraction, contraction pattern and hygroscopic expansion. *Scand J Dent Res* 90(4):329-35.

Hansen EK (1982b). Contraction pattern of composite resins in dentin cavities. *Scand J Dent Res* 90(6):480-3.

Hipwell JH, Penney GP, McLaughlin RA, Rhode K, Summers P, Cox TC, Byrne JV, Noble JA, Hawkes DJ (2003). Intensity-based 2-D-3-D registration of cerebral angiograms. *IEEE Trans Med Imaging* 22(11):1417-26.

Hofmann N, Hunecke A (2006). Influence of curing methods and matrix type on the marginal seal of class II resin-based composite restorations in vitro. *Oper Dent* 31(1):97-105.

Ilie N, Jelen E, Clementino-Luedemann T, Hickel R (2007). Low-shrinkage composite for dental application. *Dent Mater J* 26(2):149-55.

Inai N, Katahira N, Hashimoto K, Tagami J, Hirakimoto A, Marshall SJ, Marshall GW (2002). 2014 Microfocus X-ray CT Analysis of Shrinking Direction in Resin Composite. IADR/AADR, San Diego.

Jordan RE, Suzuki M (1991). Posterior composite restorations. Where and how they work best. *J Am Dent Assoc* 122(11):30-7.

Jung M, Sehr K, Klimek J (2007). Surface texture of four nanofilled and one hybrid composite after finishing. *Oper Dent* 32(1):45-52.

Kakaboura A, Rahiotis C, Watts D, Silikas N, Eliades G (2007). 3D-marginal adaptation versus setting shrinkage in light-cured microhybrid resin composites. *Dent Mater* 23(3):272-8.

Kalipcilar B, Karaagaclioglu L, Hasanreisoglu U (1991). Evaluation of the level of residual monomer in acrylic denture base materials having different polymerization properties. *J Oral Rehabil* 18(5):399-401.

Kanca J, 3rd, Suh BI (1999). Pulse activation: reducing resin-based composite contraction stresses at the enamel cavosurface margins. *Am J Dent* 12(3):107-12.

Kemp-Scholte CM, Davidson CL (1990). Complete marginal seal of Class V resin composite restorations effected by increased flexibility. *J Dent Res* 69(6):1240-3.

Kinomoto Y, Torii M, Takeshige F, Ebisu S (1999). Comparison of polymerization contraction stresses between self- and light-curing composites. *J Dent* 27(5):383-9.

Kleverlaan CJ, Feilzer AJ (2005). Polymerization shrinkage and contraction stress of dental resin composites. *Dent Mater* 21(12):1150-7.

Koran P, Kurschner R (1998). Effect of sequential versus continuous irradiation of a light-cured resin composite on shrinkage, viscosity, adhesion, and degree of polymerization. *Am J Dent* 11(1):17-22.

Kusy RP, Leinfelder KF (1977). Pattern of wear in posterior composite restorations. *J Dent Res* 56(5):544.

Kybic J, Unser M (2003). Fast parametric elastic image registration. *IEEE Trans Image Process* 12(11):1427-42.

Labella R, Lambrechts P, Van Meerbeek B, Vanherle G (1999). Polymerization shrinkage and elasticity of flowable composites and filled adhesives. *Dent Mater* 15(2):128-37.

Leinfelder KF (1993). Composite resin systems for posterior restorations. *Pract Periodontics Aesthet Dent* 5(3 Suppl 1):23-7.

Liebenberg WH (1996). Successive cusp build-up: an improved placement technique for posterior direct resin restorations. *J Can Dent Assoc* 62(6):501-7.

Lutz E, Krejci I, Oldenburg TR (1986a). Elimination of polymerization stresses at the margins of posterior composite resin restorations: a new restorative technique. *Quintessence Int* 17(12):777-84.

Lutz F, Krejci I, Luescher B, Oldenburg TR (1986b). Improved proximal margin adaptation of Class II composite resin restorations by use of light-reflecting wedges. *Quintessence Int* 17(10):659-64.

Manhart J, Chen H, Hamm G, Hickel R (2004). Buonocore Memorial Lecture. Review of the clinical survival of direct and indirect restorations in posterior teeth of the permanent dentition. *Oper Dent* 29(5):481-508.

McKinney JE, Wu W (1985). Chemical softening and wear of dental composites. *J Dent Res* 64(11):1326-31.

McLean JW, Powis DR, Prosser HJ, Wilson AD (1985). The use of glass-ionomer cements in bonding composite resins to dentine. *Br Dent J* 158(11):410-4.

Mehl A, Hickel R, Kunzelmann KH (1997). Physical properties and gap formation of light-cured composites with and without 'softstart-polymerization'. *J Dent* 25(3-4):321-30.

Meredith N, Setchell DJ (1997). In vitro measurement of cuspal strain and displacement in composite restored teeth. *J Dent* 25(3-4):331-7.

Millich F, Jeang L, Eick JD, Chappelow CC, Pinzino CS (1998). Elements of light-cured epoxy-based dental polymer systems. *J Dent Res* 77(4):603-8.

Nakabayashi N, Pashley DH (1998). Acid conditioning and hybridization of substrates. Tokyo: Quintessence Publishing Co. Ltd.

Obici AC, Sinhoreti MA, de Goes MF, Consani S, Sobrinho LC (2002). Effect of the photo-activation method on polymerization shrinkage of restorative composites. *Oper Dent* 27(2):192-8.

Ottenga ME, Mjor I (2007). Amalgam and composite posterior restorations: curriculum versus practice in operative dentistry at a US dental school. *Oper Dent* 32(5):524-8.

Palin WM, Senyilmaz DP, Marquis PM, Shortall AC (2008). Cure width potential for MOD resin composite molar restorations. *Dent Mater* 24(8):1083-94.

Park J, Chang J, Ferracane J, Lee IB (2008). How should composite be layered to reduce shrinkage stress: incremental or bulk filling? *Dent Mater* 24(11):1501-5.

Pashley EL, Tao L, Matthews WG, Pashley DH (1993). Bond strengths to superficial, intermediate and deep dentin in vivo with four dentin bonding systems. *Dent Mater* 9(1):19-22.

Pereira PN, Okuda M, Sano H, Yoshikawa T, Burrow MF, Tagami J (1999). Effect of intrinsic wetness and regional difference on dentin bond strength. *Dent Mater* 15(1):46-53.

Pfeifer CS, Braga RR, Ferracane JL (2006). Pulse-delay curing: influence of initial irradiance and delay time on shrinkage stress and microhardness of restorative composites. *Oper Dent* 31(5):610-5.

Pfeifer CS, Ferracane JL, Sakaguchi RL, Braga RR (2008). Factors affecting photopolymerization stress in dental composites. *J Dent Res* 87(11):1043-7.

Proenca JP, Polido M, Osorio E, Erhardt MC, Aguilera FS, Garcia-Godoy F, Osorio R, Toledano M (2007). Dentin regional bond strength of self-etch and total-etch adhesive systems. *Dent Mater* 23(12):1542-8.

Puckett AD, Fitchie JG, Kirk PC, Gamblin J (2007). Direct composite restorative materials. *Dent Clin North Am* 51(3):659-75, vii.

Qvist V, Qvist J, Mjor IA (1990). Placement and longevity of tooth-colored restorations in Denmark. *Acta Odontol Scand* 48(5):305-11.

Rasband WS (2005). ImageJ, U. S. National Institutes of Health, Bethesda, Maryland,

USA, http://rsb.info.nih.gov/ij/

Rees JS, Jacobsen PH (1989). The polymerization shrinkage of composite resins. *Dent Mater* 5(1):41-4.

Rösch P, Netsch T, Quist M, Weese J (2002). 3D Respiratory Motion Compensation by Template Propagation. In: T. Dohi, R. Kikins (Eds.): MICCAI 2002, Lecture Notes in Computer Science 2489:639-646.

Rösch P, Chiang YC, Kunzelmann KH (2009). Quantification of local Polymerisation Shrinkage from 3D Micro CT Images of Dental Composites. *Proceedings of Computer Assisted Radiology and Surgery (CARS); in press*.

Roulet JF, Salchow B, Wald M (1991). Margin analysis of posterior composites in vivo. *Dent Mater* 7(1):44-9.

Sahafi A, Peutzfeldt A, Asmussen E (2001). Soft-start polymerization and marginal gap formation in vitro. *Am J Dent* 14(3):145-7.

Sakaguchi RL, Sasik CT, Bunczak MA, Douglas WH (1991). Strain gauge method for measuring polymerization contraction of composite restoratives. *J Dent* 19(5):312-6.

Sakaguchi RL, Peters MC, Nelson SR, Douglas WH, Poort HW (1992). Effects of polymerization contraction in composite restorations. *J Dent* 20(3):178-82.

Sarrett DC (2005). Clinical challenges and the relevance of materials testing for posterior composite restorations. *Dent Mater* 21(1):9-20.

Schneider LF, Cavalcante LM, Consani S, Ferracane JL (2009). Effect of co-initiator ratio on the polymer properties of experimental resin composites formulated with camphorquinone and phenyl-propanedione. *Dent Mater* 25(3):369-75.

Sharp LJ, Choi IB, Lee TE, Sy A, Suh BI (2003). Volumetric shrinkage of composites using video-imaging. *J Dent* 31(2):97-103.

Sideridou I, Tserki V, Papanastasiou G (2002). Effect of chemical structure on degree of conversion in light-cured dimethacrylate-based dental resins. *Biomaterials*

23(8):1819-29.

Skrtic D, Antonucci JM (2007). Effect of Chemical Structure and Composition of the Resin Phase on Vinyl Conversion of Amorphous Calcium Phosphate-filled Composites. *Polym Int* 56(4):497-505.

Sorzano CO, Thevenaz P, Unser M (2005). Elastic registration of biological images using vector-spline regularization. *IEEE Trans Biomed Eng* 52(4):652-63.

Stansbury JW (1992). Synthesis and evaluation of new oxaspiro monomers for double ring-opening polymerization. *J Dent Res* 71(7):1408-12.

Strydom C (2005). Polymerization and polymerization shrinkage stress: fast cure versus conventional cure. *Sadj* 60(6):252-3.

Suliman AH, Boyer DB, Lakes RS (1994). Polymerization shrinkage of composite resins: comparison with tooth deformation. *J Prosthet Dent* 71(1):7-12.

Summitt JB, Robbins JW, Hilton TJ, Schwartz RS, dos Santos JJ (2006). Fundamentals of Operative Dentistry: A Contemporary Approach. 3rd edition ed. Illinois: Quintessence Publishing Co, Inc.

Sun J, Lin-Gibson S (2008). X-ray microcomputed tomography for measuring polymerization shrinkage of polymeric dental composites. *Dent Mater* 24(2):228-34.

Tay FR, Pashley DH (2001). Aggressiveness of contemporary self-etching systems. I: Depth of penetration beyond dentin smear layers. *Dent Mater* 17(4):296-308.

Tjan AH, Bergh BH, Lidner C (1992). Effect of various incremental techniques on the marginal adaptation of class II composite resin restorations. *J Prosthet Dent* 67(1):62-6.

Unterbrink GL, Muessner R (1995). Influence of light intensity on two restorative systems. *J Dent* 23(3):183-9.

vanNoort R (2007). INTRODUCTION TO DENTAL MATERIALS. 3rd ed.: MOSBY ELSEVIER.

Venhoven BA, de Gee AJ, Davidson CL (1993). Polymerization contraction and conversion of light-curing BisGMA-based methacrylate resins. *Biomaterials* 14(11):871-5.

Versluis A, Douglas WH, Cross M, Sakaguchi RL (1996). Does an incremental filling technique reduce polymerization shrinkage stresses? *J Dent Res* 75(3):871-8.

Versluis A, Tantbirojn D, Douglas WH (1998). Do dental composites always shrink toward the light? *J Dent Res* 77(6):1435-45.

Versluis A, Tantbirojn D, Pintado MR, DeLong R, Douglas WH (2004). Residual shrinkage stress distributions in molars after composite restoration. *Dent Mater* 20(6):554-64.

Watts DC, Cash AJ (1991). Determination of polymerization shrinkage kinetics in visible-light-cured materials: methods development. *Dent Mater* 7(4):281-7.

Weinmann W, Thalacker C, Guggenberger R (2005). Siloranes in dental composites. *Dent Mater* 21(1):68-74.

Wu W, Toth EE, Moffa JF, Ellison JA (1984). Subsurface damage layer of in vivo worn dental composite restorations. *J Dent Res* 63(5):675-80.

Xia Y, Zhang F, Xie H, Gu N (2008). Nanoparticle-reinforced resin-based dental composites. *J Dent* 36(6):450-5.

Yap AU, Ng SC, Siow KS (2001). Soft-start polymerization: influence on effectiveness of cure and post-gel shrinkage. *Oper Dent* 26(3):260-6.

Zanchi CH, de Carvalho RV, Rodrigues Junior SA, Demarco FF, Burnett Junior LH (2006). Shrinkage stress of three composites under different polymerization methods. *Braz Oral Res* 20(2):137-42.

CURRICULUM VITAE

Personal Background:

Name: Yu-Chih Chiang
Gender: Male
Date and Place of Birth: 21. Aug. 1973 in Tainan County, Taiwan
Citizenship: Taiwan
E-mail Address: de.ychiang@gmail.com

Education:

1979-1985	Elementary School, Liou-Jia Elementary School, Tainan County, Taiwan
1985-1988	Junior High School, Private Feng-Ho Junior High School, Tainan County, Taiwan
1988-1991	Senior High School, Private Feng-Ho Senior High School, Tainan County, Taiwan
1991-1997	D.D.S., School of Dentistry, Chung Shan Medical University, Taichung, Taiwan
2002-2005	M.S., Graduate Institute of Clinical Dentistry, National Taiwan University, Taipei, Taiwan
2005-Present	Candidate for Ph.D. in Graduate Institute of Clinical Dentistry, National Taiwan University, Taipei, Taiwan
2006-2009	Dissertation, Promotion: Zahnmedizin (Ph.D. program) at the Ludwig-Maximilians-University of Munich, Germany

Professional / Work Experience:

1996-1997	Internship, Dental Department, Chung Shan Medical University Hospital, Taichung, Taiwan
1997-1999	Compulsory Military Service
1999-2000	Resident, Dental Department, Show Chwan Memorial Hospital, Changhwa, Taiwan

2000-2002	Dentist, Private Practice Safe Dental Clinic, Taichung, Taiwan
2002-Present	National Taiwan University and National Taiwan University Hospital:

1. Adjunct Resident, Endodontic Department (*2002-2005*)
2. Teaching Fellow, Operative Dentistry and Endodontics, School of Dentistry (*2003-2006*)
3. Adjunct Attending, Endodontic Department (*2006-Present*)

2006-Present	Endodontic Specialist
2008 October	Paffenbarger Award Annual Meeting of the Academy of Dental Materials, Wurzburg, Germany. (Topic: Deformation Analysis of Composite Polymerization Shrinkage from μCT Images)

Publications:

Chiang YC (2005). Master Thesis: Mixed mode failure analysis of total-etch and self-etch dentin-resin adhesion–a fracture mechanics approach. Natioanl Taiwan University, Taipei, Taiwan.

Chen WP, Lee BS, Chiang YC, Lan WH, Lin CP (2005). Effects of various periodontal ligament elastic moduli on the stress distribution of a central incisor and surrounding alveolar bone. *J Formos Med Assoc* 104(11):830-8.

Lee BS, Chiang YC, Hung WC, Cheng JH, Lin CP (2007). Failure criteria of dentin-resin adhesion – The J-integral approach. *Scripta Materialia* 56(10):863-866.

Lee BS, Huang SH, Chiang YC, Chien YS, Mou CY, Lin CP (2008). Development of in vitro tooth staining model and usage of catalysts to elevate the effectiveness of tooth bleaching. *Dent Mater* 24(1):57-66.

Chiang YC, Lee BS, Wang YL, Cheng YA, Chen YL, Shiau JS, Wang DM, Lin CP (2008). Microstructural changes of enamel, dentin-enamel junction, and dentin induced by irradiating outer enamel surfaces with CO2 laser. *Lasers Med Sci* 23(1):41-8.

Chiang YC, Knezevic A, Kunzelmann KH (2008). Slumping during sculpturing of composite materials. *Dent Mater* 24(12):1594-601.